OCTOBER 1983

HEWLETT-PACKARD JOURNAL

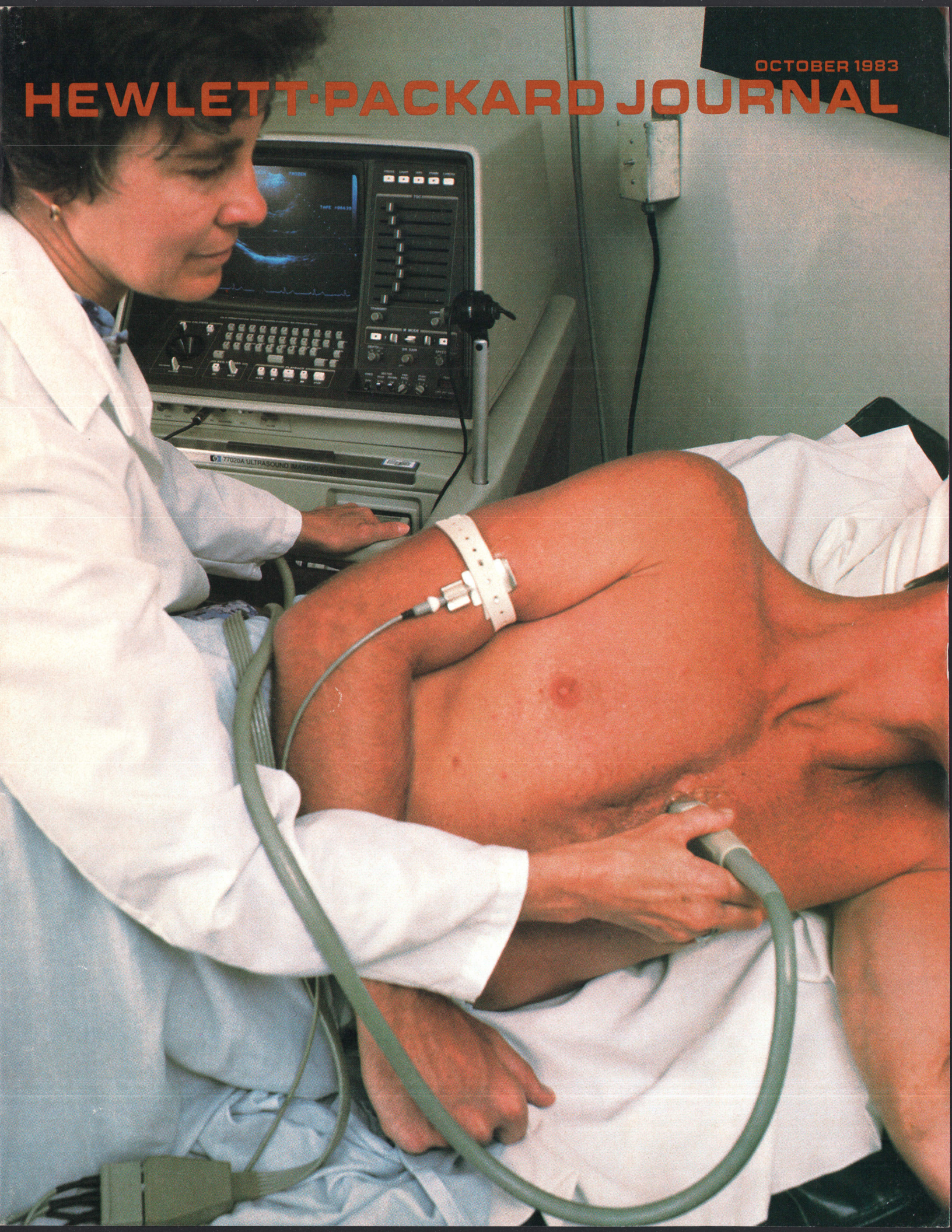

HEWLETT-PACKARD JOURNAL
Technical Information from the Laboratories of Hewlett-Packard Company

OCTOBER 1983 Volume 34 • Number 10

Contents:

In this Issue:

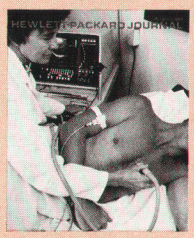

Our cover photograph shows a HP 77020A Ultrasound Imaging System being used to display a picture of a patient's beating heart. Ultrasound imaging—bouncing a series of high-frequency sound pulses off the organs and other structures inside the body—lets cardiologists, obstetricians, and radiologists see the body's inner workings without surgery and without any health risk to the patient. Heart valves and chambers can be seen in motion. A developing fetus can be observed and measured without risk. The HP system, we are told, is particularly easy to use and produces an especially high-quality image. There's no question that an enormous amount of engineering talent and effort went into its development. It's designers gave us so much interesting information that it will take nearly two full issues to publish it all. The articles in this issue discuss the system and its use, describe the design of its novel transducer (the part that touches the patient), and relate what was done to ensure image quality. On page 13, a cardiologist gives us the user's point of view. In December, we'll complete the story with articles on the hardware and software design.

-R. P. Dolan

Ultrasound Imaging: An Overview

By using a beam of ultrasound, it is possible to look at organs and other structures inside the human body without breaking the skin.

by H. Edward Karrer and Arthur M. Dickey

WHAT IS AN ULTRASOUND IMAGE? An image is a reproduction or imitation of the form of something. A major thrust of modern technology in the past century has been to enhance or complement the capability of the human sensory system with new imaging modalities. Examples that come to mind include the optical telescope, radar, sonar, infrared, and X-ray imaging systems.

The imaging process consists of two parts. First is the illumination of the objects to be imaged by some radiation. This radiation interacts with the object by means of reflection, absorption, or scattering. The second step is a reconstruction of the energy received from these interactions to form an image of the object.

The primary goal of medical imaging systems is to "see" inside the human body noninvasively. Our eyes are not useful for this since biological tissue is largely opaque to visible light. Fortunately, other forms of radiation like X-rays, some nuclear particles, and ultrasound readily pass through and interact with tissue.

Ultrasound brings several useful capabilities to medical imaging. An ultrasound image represents the mechanical properties of the tissue (i.e., parameters such as density and elasticity). Most people can immediately recognize common anatomical structures in an ultrasound image since the organ boundaries and fluid-to-tissue interfaces are easily discerned. This mechanical information complements the results of other imaging techniques, such as X-ray imaging, which displays X-ray absorption.

The ultrasound imaging process can be done in real time. This means that the viewer can follow rapidly moving structures such as the heart without motion distortion. Also, it allows the operator to move the small handheld transducer probe over the surface of the patient's body to select the proper view in an interactive way.

Ultrasound appears to be one of the safest diagnostic imaging techniques. It does not use ionizing radiation like X-ray and hence is used routinely for fetal and obstetrical imaging. There have been many studies done on the possible biological side effects of ultrasound on tissue and none has shown any harmful effects during clinical examination.

Areas where ultrasound imaging is particularly useful include cardiac structures, the vascular system, the fetus and uterus, abdominal organs such as the liver, kidneys, and gall bladder, and the eye. However, ultrasound cannot be used to image all portions of the body. Air pockets, for instance, are excellent reflectors of ultrasound and limit the penetration of sound into the lungs and bowels. Bone highly attenuates ultrasound, which makes imaging the adult brain through the skull difficult.

Physical Principles

Ultrasound generally refers to sound that has a frequency or pitch above the range of human hearing. Sound waves in human tissue are compressional (longitudinal) waves. These waves consist of repetitive or periodic regions of local compression and rarefaction which propagate through a medium at some velocity v. The spacing between successive regions of compression is called the acoustic wavelength λ. These parameters are related by the expression $v = f\lambda$, where v is the velocity in meters/second, f is the frequency in hertz, and λ is the wavelength in meters. Because it is not possible to resolve objects smaller than a wavelength, it is desirable to image at the highest possible frequency (smallest wavelength) to get the best resolution.

The most common mode of ultrasound imaging is the reflection or pulse echo mode. The analogy to radar is valid. A short burst of acoustic energy is directed into the body and the reflected energy is received at a later time. Different tissues reflect acoustic energy depending on their characteristic acoustic impedance. This impedance is defined by the expression $Z = \rho v$, where Z is the acoustic impedance in rayls, ρ is the density of the tissue in kilograms/cubic meter, and v is the velocity in meters/second.

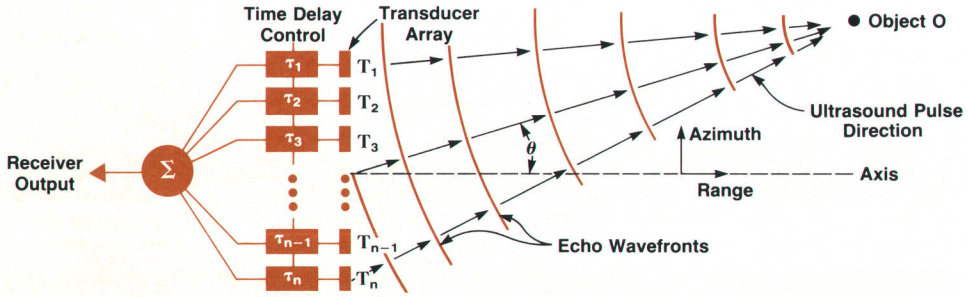

Fig. 1. *Phased-array operation of an ultrasound imaging system. By varying the delay τ_i for each transducer element electronically, the direction of the outgoing ultrasound pulse can be steered and the array can be dynamically focused on the returning echoes.*

As the ultrasound pulse passes from one tissue type to another, a portion of it is reflected in a way analogous to reflection from a discontinuity on an electric transmission line. For instance, when a pulse crosses the boundary between muscle tissue ($Z = 1.7 \times 10^6$ rayls) and blood ($Z = 1.6 \times 10^6$ rayls), about 0.1% of the acoustic energy is reflected. This echo is used to create the image of the blood-muscle interface. The rest of the pulse propagates across the interface and continues into the body to image deeper structures.

The ultrasound pulse is transmitted and received with a piezoelectric transducer. The piezoelectric material is a polycrystalline ceramic which converts an electrical signal into acoustic energy and vice versa. This transducer is the source and eye of the imaging system. It is usually placed directly on the skin surface.

As the ultrasound pulse propagates through the body, its acoustic intensity is attenuated with propagation distance. The acoustic attenuation also increases with frequency. A typical attenuation coefficient for soft tissue is 1 dB/cm/MHz. When imaging a structure that is 10 cm deep in the body at 3.5 MHz, the round-trip attenuation is 70 dB. This is an easily detectable signal when using clinically acceptable transmitter powers. Note that at 10 MHz the round-trip attenuation would be 200 dB. This points out a basic tradeoff in ultrasound imaging; as the frequency is increased to resolve finer structures, only shallow structures can be imaged. Typically, 2.5 to 3.5 MHz is used for deep abdominal imaging, 5 MHz is used for organs near the surface and in pediatric work, and 5 to 15 MHz is reserved for "small parts" imaging such as the thyroid, testicles, peripheral vascular vessels, and the eye.

Other structures can also interact with ultrasound, giving different tissues different textures. Objects much smaller than a wavelength cause Rayleigh scattering. This diffuse scattering depends on the fourth power of the frequency and the ultrasound pulse tends to scatter uniformly in all directions. Images made at higher frequencies tend to appear more "filled in" because of this effect. If an object is much larger than a wavelength, it becomes a specular reflector and acts much like a mirror.

Ultrasound Imaging Systems

B or brightness mode scanning is the most common type of ultrasound imaging. A B scan is a view of a cross-sectional slice through the object. A narrow pencil beam of ultrasound is swept through a sector to define the scan plane. The beam is formed from bursts of ultrasound. The repetition rate of ultrasound pulse generation is selected so that the transmitted pulse has time to travel to the deepest target and back again before the next pulse is launched. The pulse is assumed to travel in a straight line at a constant velocity, a good assumption in soft tissue. As the pulse propagates into the body along any scan line, echoes are generated which travel back to the receiver. These echoes vary in intensity acording to the type of tissue or body structure causing them. This data is presented on a cathode-ray-tube (CRT) display in which the brightness (hence the term B mode) depends on the echo strength. This image can be formed in real time since it takes only 260 μs for ultrasound to travel 20 cm into the body and return. If the display frame rate is 30 frames per second, 125 lines can be displayed in the image.

Ultrasound imaging systems differ in the way that the sector scan is implemented. A single transducer can be mechanically rocked or pivoted to create a sector scan. The phased-array approach uses a stationary array of many small transducers which are electronically controlled to steer and focus the beam. This concept is shown in Fig. 1.

In effect, the phased array acts like an acoustic lens with electronically variable focal length. Assume that a region of tissue at location O has reflected a small amount of an incident short pulse of ultrasound. The echo reaches each transducer element (T_i) along the array at a different time depending on the position of O. Variable time delay elements (τ_i) in series with each transducer element are rapidly varied under computer control to bring the electrical pulses generated by the echoes received at each transducer element into coincidence at the summing junction. For instance, if the object is on the axis of symmetry of the transducer array, but is far away, the returning echo wavefronts are essentially planar and the time delays are set equal. If the object is off-axis at some angle θ in the far field, the time delays must be linearly varied across the array aperture for coherent addition at the summing junction. When the object is close to the array, as shown in Fig. 1, the approaching wavefronts are more curved and the delay distribution across the array is more nearly parabolic. Changing the individual transducer delays to accommodate the curvature of the wavefronts is called dynamic focusing and is necessary to achieve maximum resolution in the near field of the array.

In a similiar manner, the outgoing ultrasound pulse can be directed to a desired location. By varying the time at which each element of the transducer array is excited by the transmitter, the direction in which the ultrasound pulses generated by each element coherently add to form one pulse can be changed from one side of the axis to the other. This is called beam steering.

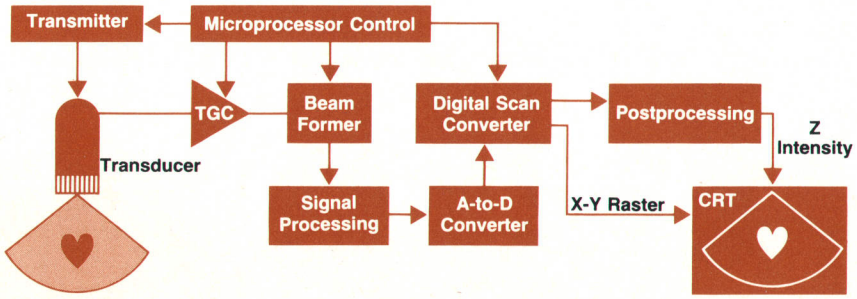

Fig. 2. *Block diagram of a basic ultrasound imaging system using a phased-array transducer.*

History of HP's Ultrasound System

by John T. Hart
R&D Manager, Andover Division

When asked to review the ultrasound project from a historical perspective, I decided to recount the highlights from what I think is the perspective of the people working on it. I hope to convey the sense of achievement and sometimes disillusionment that we all felt.

When Ed Karrer's group at HP Laboratories (HPL) took up the challenge of building a phased-array system a number of years ago, none expected that the HP 77020A would be the result. Dave Perozek, now general manager of the Andover Division, provided the initial liaison for the division, and Dr. Richard Popp from Stanford University Hospital provided the clinical guidance. Many layers of the onion had to be removed before we met our performance goal. The first system was improvised, and occupied half the area of a large room, but the reaction to the images was genuine excitement. On the TV screen was a picture of John Larson's beating heart. That was the impetus to form a section at the Andover Division to develop the technology and build a new product line.

While the first images provided a very real likeness, they were overlayed with "ghost" images. This artifact was caused by grating lobes, in turn caused by sparse transducer array spacing, since there were only 16 elements. To eliminate this, it was necessary to have 64 elements in the transducer, spaced one half wavelength apart. This was discouraging because it was just too costly to have that many receiver channels, each with its own delay line. Fortunately, however, Sam Maslak had designed a mixing capability into the first system which would allow small time delays to be approximated by phase shifts. In two months, it was tried and found to work. It was possible to build a 64-element system at reasonable cost and eliminate the grating lobes causing the ghost images.

It was at this point that the promise of a high-performance cardiology system at substantially lower cost became apparent. There were a few real-time ultrasound systems in the marketplace at that time which clearly demonstrated the advantages of real-time ultrasound, but they were expensive and the picture quality was far from optimal. With lots of determination and the promise of a real advance, we undertook a joint HPL/Andover Division effort to build a new system.

The initial Andover organization was small. Arthur Dickey was project manager for the scanner, transducer and scan converter. Larry Banks was responsible for system integration and control. As the project grew in size, Jim Fearnside took on the task of managing the transducer development, Ray O'Connell the display and scan converter, and Tony Vallance the system software. I was the section manager.

Sam Maslak worked with the scanner team to design the beam steering electronics. This was to be driven by HP's custom 16-bit silicon-on-sapphire microprocessor instead of the original minicomputer. HPL had to carry the ball in developing the 64-element transducer as Andover had neither the facilities nor the expertise to do it. The highest priority was to develop the scanner and transducer, because that was where the basic improvement in image quality would be derived. Also, our theories had to be tested in practice. After considerable work, there was initial success, mixed with more disappointment. The images showed that the grating lobes were eliminated, but the images were filled with clutter and had lower resolution than expected.

The solution required extensive reshaping of the acoustic beam, elimination of spurious transducer modes, and careful control of the frequency spectrum. Hugh Larsen and Rick Pering were able to model the design parameters and calculate the new design constraints. Art Dickey and Ron Gatzke rose to the challenge, squeezing out significant performance improvements in the scanner, while Bob McKnight was given the difficult assignment of optimizing the video processing chain. Jim Fearnside and John Larson provided some innovative solutions to our transducer problems, while Dave Miller contributed in the complex area of acoustic lens design.

The image quality got another boost from Hugh Larsen and Steve Leavitt who invented the R-Theta scan conversion algorithm. Barry Hunt joined in this effort at a later time and made significant contributions. This scheme makes it possible to achieve artifact-free reconstruction of the ultrasound image in television video output. The Nyquist criterion as it relates to the acoustic line density indicated that this could be achieved, but up until this time all real-time sector ultrasound images were plagued with a steppy or jagged appearance because of the necessarily simple approximations made in calculating a picture "on the fly." The 77020A system demonstrates a display in which such discontinuities are almost imperceptible.

In parallel with this effort to improve image quality, Pete Rhoads, in charge of industrial design, and Larry Banks were subjecting the package design and human interface to clinical trials. Here, the 60-Hz CRT display and the peripheral devices such as the video cassette recorder and the stripchart recorder presented a particularly important challenge, because the images that the user sees must come through all of these devices. It turned out that none of these problems was easy to solve, because the eye is amazingly sensitive to even the slightest inaccuracy in gray scale or position. John Dukes at HPL had discovered some of the gray-scale mapping problems in the earlier HPL system and had done some preliminary work to quantify these complex problems. Al Tykulsky, assisted by Jan Accettura, worked out the problems in the 60-Hz display. Steve Leavitt, Jim Mniece, and later Alwyn D'Sa solved the problems in the digital video interfaces. Jim Conrad and later Rich Jundanian worked out the interfaces involved in putting images on the stripchart recorder.

The human interface also received a great deal of attention during the clinical trials. Within the 77020A, there are multiple 16-bit microprocessors, each operating its own subsystem. It is important in a clinical environment that the operation be obvious and natural, and that the system recover from errors easily. This presented a significant challenge to the software design teams. Joe Luszcz and Bill Koppes made significant contributions to the overall software system design and the implementation of an effective and reliable real-time operating system. Definition and implementation of the scan converter architecture was done by Dave Hempstead, while definition and implementation of the scanner software was done by Al Langguth and Bob Kunz. The high-speed communication of data between these subsystems required careful definition of architecture and communication protocols and was an excellent example of the cooperative team effort that characterized the project.

Testing and servicing the 77020A System were equally complex and challenging because so many new technologies were being introduced simultaneously. Radhu Basu, Tom James, and later Tony Vallance and Al Langguth each made real contributions to the test plan and in managing its implementation. Tony Fisher designed an innovative automatic transducer test system for beam plots and individual element characterization, permitting the manufacture of consistently high-quality trandsucers. Gary Seavey and Tom Szabo worked out many of the problems involved in characterizing the transmitted acoustic power. This is especially important, since the "object" under examination is a human being.

Continued work has further improved system performance since its initial introduction. Several 3.5-MHz and 5.0-MHz transducers, which significantly improve image quality, have been added to the product line. Quarter-wave matching technology has been developed to increase transducer sensitivity, permitting these probes to be used on most patients. Jim Fearnside, Dave Miller, and Jerry Leach played the key roles in developing these transducers. Tom Szabo developed a more accurate model for transducer elements which speeded up the development of these transducers and gave us a tool that accurately predicts the performance of new transducer configurations.

Ron Gatzke's scanner group, notably Rick Snyder, Syd Karp, and Jim Conrad, gave image quality another boost by increasing the number of transmitters to 64 and reshaping the beam and the gray scale. A new image processing team, headed by Paul Magnin, has been chartered to find even more ways to improve the very important parameter of image quality.

Along with higher performance, a broader range of peripherals and system enhancements such as Rachel Kinicki's quantitiative cardiac and obstetric analysis packages have provided a high-performance, attractive, mobile, and easy-to-use system.

There were many others without whom the project could not have been completed. In all, there were well over 100 people actively involved, including the printed circuit design and fabrication teams and the manufacturing engineers who were engaged in the design and development of the processes and the product.

The HPL and Andover Division development teams have designed the highest-performance cardiology ultrasound system available today, and perhaps more important, have put into place a solid base of technology and application understanding on which we can extend the use of diagnostic ultrasound into new areas of health care.

In practice, the transmit and receive functions are separate. Consider the events necessary to generate one line of the image. First, a set of ultrasound pulses is launched so as to provide a coherent wavefront along a given scan direction. This beam is focused at midrange. As the transmitted wavefront propagates into the body, it is scattered by objects along the scan line and echoes start returning to the array. In the receive mode, the array continuously changes its focus as echoes are received from successively deeper regions. This dynamic focusing process allows an array with an aperture of 2 cm to have a varying depth of focus from 2 to 20 cm.

Resolution is the ability to separate small objects in the scan plane visually. It has three components: range resolution (along a scan line), azimuth resolution (perpendicular to a scan line within the plane of the sector scan), and

elevation resolution (the thickness of the sector scan slice). The range resolution is determined by the ultrasound pulse length. A shorter pulse gives higher resolution. The pulse length is primarily determined by the system bandwidth. Two targets 0.75 mm apart in range can be resolved with a 1-μs ultrasound pulse (3 cycles at 3.5 MHz).

The resolution in the azimuth direction depends on the array aperture (length of the array) and the acoustic wavelength λ. The principles are the same as for an optical telescope. High azimuth resolution is achieved with a large aperture and a short wavelength. Dynamic focusing optimizes the azimuth resolution of the imaging system.

A block diagram for a general ultrasound imaging system is shown in Fig. 2. The transmitter excites the transducer elements with short electric pulses so that a burst of ultrasound is generated. The returning echoes are applied to a variable-gain stage in the receiver called a time gain compensation (TGC) amplifier. This amplifier increases its gain with time, thus compensating for tissue attenuation as echoes come from deeper regions of the body. In a phased-array system, each element of the transducer has its own TGC amplifier. The beam former combines the outputs of the individual receiver channels by using variable time delay and phase adjustment to bring the received signals into coincidence and hence bring an object into focus. Since the received echoes have a very wide dynamic range, the signal processing stage uses signal level compression. For instance, when imaging the heart, the strong echo from the posterior wall of the left ventricle can be 50 dB greater than the diffuse echoes from the endocardial tissue. This data must be compressed to be compatible with the 25-dB dynamic range of normal CRT displays. The compressed signal is then converted from analog to digital form so that an entire image frame can be stored in the memory of the digital scan converter. The digital scan converter changes the scan format from a sector display to a conventional television raster scan. It also permits digital postprocessing of the images. These various activities—the transmitter, TGC amplifier, beam former, scan converter, and display—are coordinated under microprocessor control.

An Ultrasound Imaging System

This instrument views the internal organs and tissues of the human body in real time by directing a beam of short ultrasound pulses into the body and then receiving and processing the acoustic echoes to form a displayed image.

by Lawrence W. Banks

THE HP 77020A ULTRASOUND IMAGING SYSTEM (Fig. 1) is a real-time phased-array imaging system offering a 90° sector image constructed with a polar-to-rectangular conversion algorithm that minimizes artifacts in the image. The operator can select either a sector-only display or a small-sector display with one or two M-mode traces. The system provides the operator with a variety of capabilities which include stop action, hard-copy reproduction, and quantitative analysis.

Product Goals

Developing a system of this size and complexity requires a clearly defined list of goals. From several marketing studies came these five: real-time imaging, phased-array architecture, high image quality, mobility, and ease of use.

Without the ability to image and display in real time (30 Hz), the system would not address the needs of the cardiologist to visualize the heart, especially its valves. Although not required in radiology applications, real-time scanning increases the speed of the examination and leads to better and more cost-effective diagnosis.

The second goal was a phased-array electronic architecture. Of the three basic real-time imaging technologies, mechanical, linear, and phased-array, the last is the most complex, but allows the most versatility and combines the advantages of the other two. Phased-array systems use a small and reliable transducer that can transmit and receive acoustic energy through the space between the ribs. This gives a sector format with a large field of view, allowing the full adult heart to be imaged.

The most elusive and hardest to define goal was image quality. Although easy to quantify from engineering concepts of acoustic beamwidth, signal-to-noise ratio, pulse length, etc., defining what a doctor "sees" is far more difficult. In fact, different types of doctors such as cardiologists and radiologists view images differently.

In 1976, state-of-the-art ultrasound systems were either early attempts at real-time systems with limited image quality or brightness (B) scanners. The images from these systems looked very different and yet together satisfied the needs of doctors at that time. Our goal was to exceed the image quality of the single-frame B scanners and improve the features of the real-time systems.

Most systems available during this period were large and

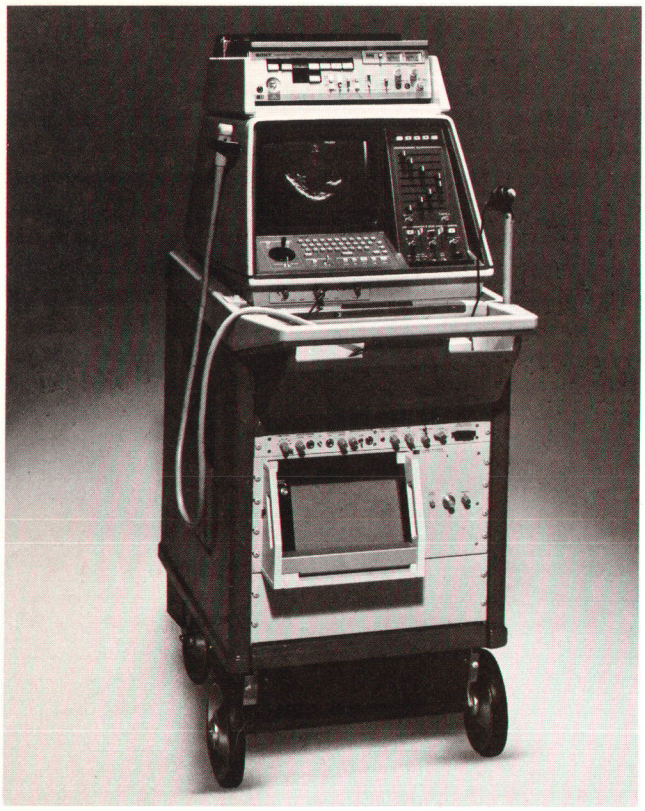

Fig. 1. *HP Model 77020A Ultrasound Imaging System provides both M-mode and two-dimensional sector scans of human tissue for cardiac, obstetric, and abdominal examinations. The system is mounted on a mobile cart in a configuration for rapid and easy use.*

difficult to move throughout the hospital. To allow use in intensive care and coronary care units, the 77020A had to be small and mobile, the fourth goal.

An easy-to-use system is also important in medical applications. This became the fifth major goal. Many systems were "stacks of boxes" with controls scattered everywhere. The 77020A centralizes all controls on panels surrounding the display, allowing the diagnostician to concentrate on the diagnostic information in the image rather than on these controls.

To guarantee that the system would be easy to use, all hard-copy, display, and storage modules have matching gray-scale images. This requires proper gamma correction for each medium. Although a simple concept, many copies can be wasted trying to get a good hard copy of the video image on the monitor. Slight differences in gray-scale linearity can subtly but significantly change the appearance of the image.

To guarantee friendliness, the system was designed from the outside in. The human interfaces, including display formats and control panels, peripheral locations, size, and weight were all determined based upon human rather than technical requirements. Although this made the engineering requirements more difficult, it helped solve the doctor's problem.

System Controls

The 77020A System is controlled by the operator through three control panels. The vertical panel to the right of the display contains the controls needed for normal imaging and peripheral control. The sector imaging controls include the major controls for generating the ultrasound image. The TGC (time gain compensation) controls used to compensate for the acoustic attenuation of the human body allow the operator to optimize the image by adjusting the gain of the receivers for different depths.

The **TRANSMIT** and **COMPRESS**ion knobs control the transmitted power of the system and the video compression of the image. The **DEPTH** selector adjusts the maximum imaging depth to 4, 8, 12, 16, 20, or 24 cm, while the **SPEED** selector allows an M-mode trace speed of 10, 25, 50, or 100 mm/s on both the display and the stripchart recorder. The final imaging control is the **FREEZE** button used to store the current image in the digital scan converter's memory.

M-mode imaging along a selected sector display line is controlled by the group of controls in the lower center of the vertical panel. The paddle switches in the center of the **M-MODE** area select the particular acoustic line. Two lines can be displayed at once (M1 and M2). The center paddle switch allows any 8-cm segment of the two lines to be selected as an M-mode "zoom." The M-mode image format is selected by two pushbuttons which toggle the M-mode traces on and off.

The pushbuttons at the top of the vertical panel control the various peripherals. The **CAMERA** button takes a picture on the video camera. The **FRAME** button freezes an image and then sends the frozen image to the stripchart recorder. The **TAPE** button enables the video cassette recorder's record function. The **CHART** button runs the stripchart recorder for normal operation in M-mode. The **CHART**, **TAPE**, and **FRAME** functions are repeated on a footswitch, allowing hands-off control of these functions.

The setup controls hidden under a door (shown open in Fig. 1) at the bottom of the panel are used to customize the system for a particular image. The two **SECTOR** switches set up the system for the type of organ being imaged. The **VIDEO** switch allows either white on black (**W/B**) or black on white (**B/W**) imaging. The **PRE-PROC**essing switch allows a choice of four different analog video processing options. The **POST-PRO**cessing switch selects four different digital gray-scale processing options. The **TEST** switch and five-digit hexadecimal display are used for the internal resident test software.

The horizontal panel below the display contains all the necessary controls to annotate the image during real-time scanning, play back the image from a video cassette recorder (VCR), trigger the image from an ECG waveform, and analyze the image. The alphanumeric keyboard is used to enter patient ID and other data onto the image.

The controls available on the horizontal panel to configure the system or analyze images are generally used when the patient is not being scanned. The left part of the panel includes a joystick to allow the operator to measure lengths, areas, and volumes of two-dimensional images, and heights, times, and slopes of M-mode traces. The ▼ and ▲ buttons select which end of the cursor is enabled for move-

Quantitative Analysis for Ultrasound Imaging

by Rachel M. Kinicki

It is often necessary to supplement the qualitative anatomical and functional information obtained during an ultrasound examination with quantitative measurements and derived calculations. Since cardiologists and obstetricians, in particular, rely heavily on quantitative information obtained from ultrasound images, two analysis packages were added to the HP 77020A Ultrasound Imaging System to meet their needs. These packages provide measurement capability via the system calipers to measure desired parameters accurately, perform standard calculations based on these measurements, allow for input of patient history data and comments, and generate a hard-copy report that summarizes the data.

Cardiac Analysis

The ability to assess ventricular function is one of the most important applications of ultrasound in cardiology. To distinguish abnormal from normal heart functioning, the left ventricle, in particular, is studied thoroughly using measurements and derived calculations. Linear dimensions such as chamber diameters, wall thicknesses, and valve separations are determined as well as cross-sectional chamber areas. Derived quantities, such as left ventricular volume, stroke volume, and cardiac output, are calculated from these measurements.

The heart's left ventricle pumps blood returning from the lungs to the rest of the body. Changes in left ventricular blood volume over the heart cycle are an indication to the cardiologist of the ventricle's functioning ability. M-mode and two-dimensional imaging techniques provide one- and two-dimensional measurements respectively, but volume is a three-dimensional quantity. Much research has been done on accurately computing left ventricular volume from these measurements and this has led to modeling the left ventricle as a geometric figure or combination of figures. For example, the bullet formula assumes the ventricle is shaped like a combination of a hemisphere and a cylinder and the modified Simpson's rule formula assumes the shape is a combination of a cylinder, a truncated cone, and a cone. The cardiac analysis package offers the operator a choice of six of the most accepted techniques for calculating left ventricular volume.

Obstetric Analysis

The obstetrician uses ultrasound as a tool to determine fetal viability and to monitor fetal development. The gestational sac can be identified with ultrasound by the end of the fifth menstrual week (fetal gestational age is most often computed from the first day of the mother's last menstrual period). By the seventh menstrual week, the fetus can be recognized and a pulsating heart can be seen. As the fetus develops, ultrasound reveals fetal anatomy, placenta development, and uterine structure.

Much research has been done to correlate fetal anatomical dimensions with fetal age and weight. Fetal age determination is probably the most important information available to the obstretrician since it is used to detect normal versus abnormal growth. One of the most accurate ultrasound techniques for determining fetal age is to measure the fetal crown-rump length in the first trimester of pregnancy when biological variation between fetuses is usually small. The crown-rump length is the longest length of the fetus excluding the limbs. Several researchers have measured this length when the gestational age was known and have established tables or formulas that can be used to verify age from this measurement. In the second and third trimesters, the crown-rump length becomes too large to be completely seen, so measurements such as the fetal biparietal (head) diameter and femur length are used to determine fetal age. These measurements, together with abdominal measurements, can be used to estimate fetal weight and to investigate the possibility of intrauterine growth retardation which may indicate that the fetus is not receiving proper nourishment.

Analysis Packages

Two philosophies of how analysis packages should work were discussed when designing the on-line analysis packages for the 77020A. The first approach can be called the walk-through method; the operator is prompted for all measurements in a predetermined sequence and must either make each measurement or skip over it before continuing with the next. The second philosophy is to allow free-form input of measurement data. This method allows the operator to input measurements in any order. It is the operator's responsibility to enter all of the necessary

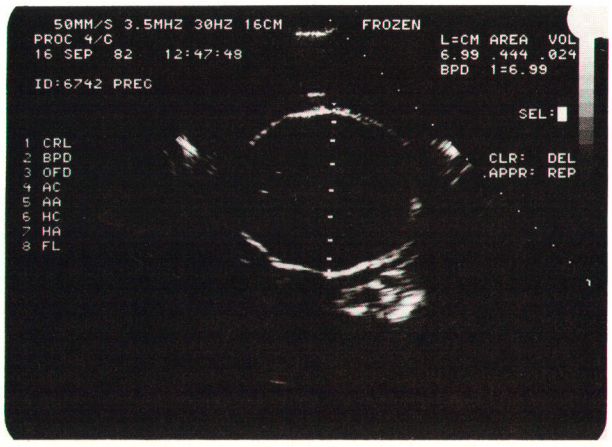

Fig. 1. *Obstetric analysis package measurement menu with fetal biparietal diameter measurement stored.*

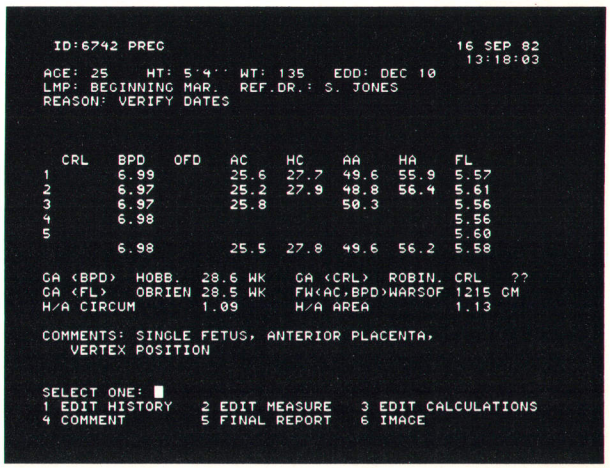

Fig. 2. *Sample edit report for obstetric analysis package.*

measurements during the course of the study. The HP analysis packages are implemented using the philosophy of free-form measurement input. Although the walk-through method might be better for inexperienced operators, it can be very frustrating to the experienced operator who prefers to make measurements in a logical (perhaps anatomical) order that differs from the package measurement order. This frustration is particularly noticeable in obstretrics since the fetus is often quite active and good images for measurements are not easy to obtain in any defined order. The analysis packages are also available during video tape playback so free-form input helps to eliminate unnecessary tape searching that would be required to find the current measurement asked for by the walk-through method.

The operator gains access to the quantitative measurement packages by pressing the **ANALYSIS** key on the 77020A's keyboard. Upon entering **ANALYSIS** mode, a menu is presented to the operator which associates a measurement number with the measurement name and identifies the special function keys (see Fig. 1). An operator prompt message, SEL:■, is also printed on the screen. To store a measurement as analysis package data, the operator positions the system calipers by pressing the **CALIP 2** key and using the joystick, and then typing the number associated with the measurement. When the numerical key is typed, the system stores the value indicated by the calipers into memory as one value for that parameter and the value is displayed on the screen below the caliper values. Several values for each measurement can be stored and the average of these is used by the system when performing the analysis package calculations.

After measurements are made, the operator presses the **APPROVE** key. The display is cleared and the operator is presented with the analysis package edit report (see Fig. 2). This report contains patient identification, time and date, patient history, all stored measurements and their averages, the configured calculations, and comments. A menu of commands gives the operator the ability to modify the report as needed.

Two sections of the edit report are reserved for qualitative information about the patient and the examination. The patient history section of the report contains configurable prompt headings followed by enough space to insert the appropriate information. This section contains relevant patient information such as age, height, and weight. The EDIT HISTORY menu command is used to add or modify the values associated with each heading. The COMMENTS menu command can be used to enter three lines of text summarizing the findings for this particular patient.

The quantitative information is summarized in the measurement and calculation sections of the edit report. These sections are dependent upon one another since the calculated values are computed by the ultrasound system from the appropriate average measurement values. When the operator selects the EDIT MEASURE command, the operator can add, modify, or delete measurements as needed. Any edited measurements are marked with an asterisk to indicate that the value was manually entered and not measured by the system. When the operator is finished editing measurements, the measurement averages and calculations are recomputed and redisplayed.

The operator may wish to edit the calculation values for several reasons. Calculations that are irrelevant for the current patient can be deleted. The operator may wish to use a calculation formula that is unavailable in the obstetric package; editing allows the operator to compute the value and type it in the appropriate space manually. In the cardiac package, a different volume algorithm can be selected for the calculation if the operator feels that it is more appropriate for the current patient than the configured one. Selecting the EDIT CALCULATIONS menu command allows the operator to edit the calculation values or change a volume method. Any edited values are marked to indicate that they were edited and not computed by the system.

After any necessary editing is completed, the operator has two choices. If it is felt that more measurements should be made, the operator can return to real-time imaging or tape playback by choosing the IMAGE menu command. All stored measurements, history, and comments are retained and any new measurements are appended to the report. If the operator is satisfied with the contents of the edit report, the operator selects the FINAL REPORT command from the edit report menu. The screen is updated with the final version of the report. The final report differs from the edit report in that only the average values for each of the measurements are displayed and it is reformatted slightly for aesthetic reasons. No edits can be made to this report. Any of the system hard-copy devices can be used to make copies of the final report for filing purposes.

The analysis packages are complemented by the SYSTEM CONFIGURATION command. This command allows the operator to choose certain system parameters and analysis package features. Menus are used to configure the analysis package features. One menu allows the operator to select from a list of available calculations the ones the system will perform automatically. Another menu allows the operator to configure the patient history headings as appropriate for the particular department using the analysis package. The configuration data for each analysis package is stored separately in system memory to allow for differences between the two packages.

ment with the joystick (see Fig. 1 on page 8). The paddle switch changes the size of a displayed ellipse and allows measurement of an area or volume (the ellipse rotated around the cursor axis).

The **CALIPer 2** key freezes the current set of measurements and enables a second set. After the second set is enabled, the **CALIP 2** button toggles between the two sets, leaving both lines or ellipses on the screen. **ANALYSIS** allows image analysis using the internal obstetric or cardiac analysis software (see article on page 8). **SET TIME** allows the internal calendar clock to be set to the current date and time. This data, along with all other setup data, is stored during power-down conditions in nonvolatile RAM.

SECTOR SIZE switches the size of the sector on the monitor from normal to large, allowing the diagnostician to see more detail in the image. **CONF** puts the system into a configuration mode, which allows the doctor to customize the system for the hospital's needs.

System Description

Fig. 2 shows a block diagram of the 77020A. Based upon the particular transducer, the depth setting, and whether M-mode is selected, the pulser and timing section of the scanner generates 64 different transmit pulses, each at the proper frequency and phase to steer the acoustic beam in the desired direction. These are amplified by the drivers to the level determined by the transmit control, and transduced into acoustic energy by the transducer array.

The echoes detected by the transducer have about 115 dB of dynamic range. Displaying this information to the observer who, at best, has a limited visual dynamic range of 25 dB, requires much processing. First, the TGC settings

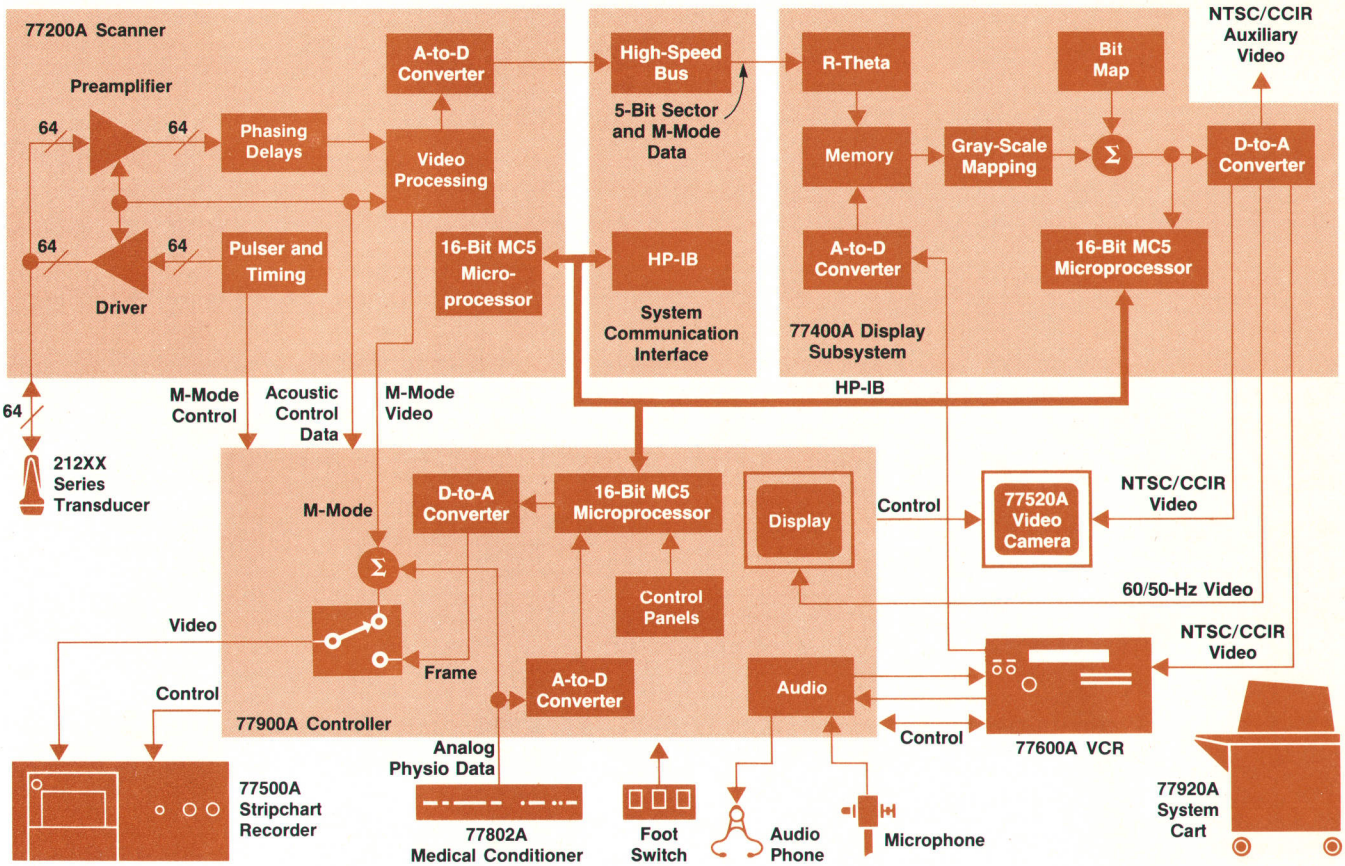

Fig. 2. *Block diagram of the 77020A Ultrasound Imaging System.*

applied to the 64 preamplifiers window an appropriate 55-dB segment of the returning signals. This data is then combined in the phasing delays to generate the video signal. Based upon the operator settings of the **COMPRESS**, **SW GAIN**, and **PRE-PROC** controls, this video signal is processed and sent to the stripchart recording interface circuits in the controller for paper-trace hard copy and to the display subsystem.

Before it is presented to the display subsystem, this data can be intercepted by an HP 1000 Computer for analysis or tissue identification studies. Allowing this to happen before scan conversion of the acoustic data gives the system the capabilities of real-time data capture without any of the data reduction problems that conversion to standard NTSC/CCIR video generates. The raw RF acoustic data can also be captured.

This data now enters the digital scan converter where it is converted from the acoustic data's polar coordinates to raster-output Cartesian coordinates using a special conversion algorithm to remap the data (see article on page 30). Stored in a 480×640 five-bit display memory and postprocessed (gray-scale mapped) as selected by the operator, the data is summed with graphic/character data from the bit map and converted to video for display on the high-speed display in the controller, storage on the VCR for later playback, transmission to any standard video auxiliary device, or transmission to the video camera for hard-copy output.

The high-speed display in the 77900A Controller was especially developed for 60-Hz noninterlaced (flicker-free) video, gamma-corrected for the human eye. The controller is the node for both control and peripheral data conversion. All control, hard copy, and storage data is routed through this instrument to allow simple, cost-effective updates. The control panels are also part of the controller.

To allow full gray-scale control of the video playback from the VCR, the image is converted from analog to digital data and read back into the memory. Audio data such as the doctor's verbal comments or diagnostic heartsound data is also stored and played back through this system.

Stripchart recording of gray-scale data requires a fiberoptic oscillographic recorder. This normally is used for M-mode hard-copy output. When the operator wishes to add a full-frame image to the M-mode stripchart recording, data can be routed via the internal HP-IB (IEEE 488) from the digital scan converter memory through the controller to the stripchart recorder. This data is also gamma-corrected for the dry-silver media used by the recorder so that the hard-copy image matches the display. The operator also has the option of adding physiological data such as electrocardiograms to the image or hard copy for timing and additional diagnostic information.

Acknowledgments

In a development effort of this magnitude, there are far too many people to be listed. A few must be. Dave Perozek,

R&D functional manager during the development and presently general manager of HP's Andover Division, was steadfast in allowing us the freedom to pursue the level of quality achieved. John Hart, the ultrasound section manager when the project was started and present R&D functional manager, became mentor to all of us, never accepting anything but the best and helping many of us to grow both technically and personally. I would like to thank Joe Luszcz for his constant and hardworking efforts toward developing the original software used in the clinical trials and his management of the system software group, and Ken Klipple, the system hardware engineer during the final development phase and now product assurance engineering manager, for always being able to find the time to solve one more system problem.

Finally, a special thanks to Pete Rhoads, manager of industrial design at Andover, who has the capacity to assimilate technical constraints and invent human solutions for friendly design, for being the driving force behind the innovative packaging and controls.

Authors

October 1983

3

H. Edward Karrer

With HP since 1966, Ed Karrer has made contributions resulting in five patents related to sensors and transducers and fifteen papers on acoustic imaging, SAW devices, sensors, and quartz resonators. He was manager of the physical acoustics department of HP Laboratories before assuming his current responsibilities as manager of the medical department. Ed studied electrical engineering at Stanford University and received a BSEE degree in 1959 and an MSEE degree in 1960. He is a Senior Member of the IEEE and a member of the American Institute of Ultrasound in Medicine. Born in Brentwood, California, he is married and the father of two teenage children, and lives in Palo Alto, California. Outside of work he enjoys fishing and playing and teaching classical guitar.

Arthur M. Dickey

Art Dickey joined HP in 1975 with ten years' experience in communications systems engineering and project management. Born in Lynn, Massachusetts, he attended Worcester Polytechnic Institute and received a BSEE degree in 1965. Further study at Northeastern University earned him an MSEE degree in 1969. At HP he managed the ultrasound scanner project and currently is the section manager for ultrasound systems. He is a member of the IEEE, lives in North Andover, Massachusetts, and is married and the father of three children. Outside of work, Art enjoys competitive sports, particularly softball and racquetball.

6

Lawrence W. Banks

Larry Banks joined HP in 1969 as a project engineer working on cardiographs. He currently is a project manager for ultrasound system hardware. Born in Stratford, Connecticut, Larry was educated at the Massachusetts Institute of Technology, earning a BSEE degree in 1967, an MSEE degree in 1969, and the Electrical Engineer degree in 1970. He is a member of Sigma Xi and is active in city government activities in Burlington, Massachusetts, where he lives with his wife and two daughters. Outside of work he is interested in astronomy, personal computing, carpentry, photography, and tennis.

8

Rachel M. Kinicki

A development engineer at HP's Andover Division since 1980, Rachel Kinicki worked on the analysis packages and the controller tests for the 77020A. She currently is working on off-line image analysis. Rachel received her education at Wake Forest University, earning a BS degree in mathematics in 1976, and Duke University, earning an MSEE degree in 1977 and a PhDEE degree in 1979. She is a member of the IEEE, is involved in local church activities, was born in Athens, Georgia, and now lives in Acton, Massachusetts. She is married and recently had her first child, a son. Her interests include swimming, gardening, sewing, and needlecrafts.

13

Richard L. Popp, M.D.

Richard Popp is the Associate Chairman of the Department of Medicine, Stanford University Medical Center. His other responsibilities include being Professor of Medicine, Cardiology Division, Medical Director of the Echocardiography Laboratory, and clinical care, investigation, and teaching. He received the AB and MD degrees from Johns Hopkins University and did his internship and residency in internal medicine there. He also completed a residency in internal medicine and a fellowship in cardiology at Indiana University, and a fellowship in cardiology at Stanford University Medical Center. Dr. Popp is a past president and a current board member of the American Society of Echocardiography, past secretary, current board member, and Fellow of the American Institute for Ultrasound in Medicine, Fellow of the American College of Cardiology, a member of the Council on Clinical Cardiology of the American Heart Association, and a member of the American Society for Clinical Investigation.

17

John D. Larson III

John Larson is a native of Oregon, educated in Boston at the Massachusetts Institute of Technology, and transplanted to California where he studied at Stanford University to receive a PhDEE degree in 1971. After a year of postdoctoral work at the Technical University of Denmark, he joined HP Laboratories in 1972. A project manager for diagnostic imaging, his contributions in microwaves, acoustics, and process development have resulted in three patents and over 20 publications. John is a member of Sigma Xi, a Senior Member of the IEEE, and chairman and cofounder of the Santa Clara Valley IEEE group on sonics and ultrasonics. In his spare time he has been involved with several civic activities such as school play-

ground construction, the Cub Scouts, and church leadership. He is married and the father of two children. His favorite pastimes include jogging, hiking, and outdoor sports.

22

David G. Miller

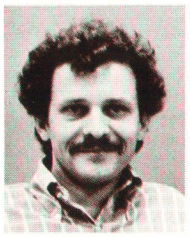

Dave Miller was born in Ogden, Utah, and attended the University of Utah where he received a BSME degree in 1967. He then joined HP and worked on recording devices and the 47201A Oximeter. His contributions have resulted in three patents related to ultrasound transducer design. He lives with his wife and two boys on their developing farm in Boxford, Massachusetts. An avid do-it-yourselfer, he built their passive solar and wood-heated home, where keeping warm during the New England winters is an adventure. He enjoys cross-country and downhill skiing.

24

George A. Fisher

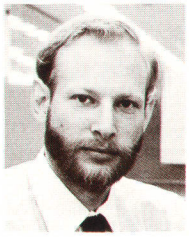

Born in Framingham, Massachusetts, Tony Fisher studied physics at Southeastern Massachusetts University (BS, 1976) and ocean engineering at the University of Rhode Island (MS, 1978). He then joined HP as a production engineer and worked on manufacturing and component improvements before assuming his current position as an R&D engineer. He is the author of two papers on evaluating acoustic parameters. In his free time Tony enjoys scuba diving, personal computing and photography. He lives in Andover, Massachusetts.

26

Thomas L. Szabo

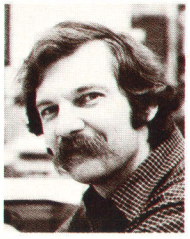

Tom Szabo joined HP in 1981 with several years of experience as a research physicist. He is the author or coauthor of over 60 papers related to ultrasonics, SAW devices, nondestructive testing, and transducer design. His work has resulted in three patents. At HP he has worked on transducer design and now is concerned with image quality R&D. Tom was born in Budapest, Hungary and was educated at the University of Virginia (BEE, 1966) and the University of Rochester (MSEE, 1968). He is a member of the IEEE, the Acoustical Society of America, and Sigma Xi. Living in Newburyport, Massachusetts, he is interested in travel, cycling, training cats to do tricks, and photography (he currently is completing an album of gargoyle photos).

Gary A. Seavey

With HP since 1963, Gary Seavey contributed to the development of the cesium beam tube and rubidium frequency references. This work resulted in three papers, one of which appeared in the HP Journal. He currently is a project engineer at HP's Andover Division. Gary holds a BS degree in physics awarded by the University of Santa Clara in 1971 and is a member of the American Vacuum Society. Born in North Conway, New Hampshire, he now lives in Boxford, Massachusetts where he is a member of the volunteer fire department. Gary is married, has two children, and enjoys tennis, racquetball, and swimming.

30

Steven C. Leavitt

A native of Portland, Maine, Steve Leavitt holds a BSEE degree awarded in 1971 by the University of Maine. He joined HP in 1978 with six years of experience with communication systems. He currently is working on digital hardware designs for ultrasound instruments. Steve is coauthor of a paper on the 77020A's R-Theta algorithm, and is a member of the IEEE. He served four years in the U.S. Air Force, is married, and lives in Hampstead, New Hampshire. During his free time, he enjoys mountain climbing, hiking, and bicycling.

Barry F. Hunt

Barry Hunt studied computer systems engineering at the University of Massachusetts at Amherst and received a BS degree in 1977. After two years working on microprocessor system design for a government contractor, he came to HP in 1979 and worked on the digital design of the 77020A's scan converter. Born in Chicopee, Massachusetts, he is married and lives in Nashua, New Hampshire. He enjoys working with home computers and playing golf and softball.

Hugh G. Larsen

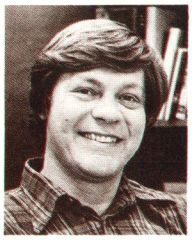

Hugh Larsen received his education at Brown University (BSEE, 1965), the University of Cincinnati (MSEE, 1971), and the University of Vermont (PhDEE, 1976). He also worked for a computer systems manufacturer during the late 1960s. He joined HP in 1976 and worked on algorithms for the 5600C ECG Analysis System and many aspects of the 77020A Ultrasound Imaging System, in particular the scan conversion algorithm and image quality. His contributions have resulted in seven papers on spectral estimation, dynamic membrane analysis, and Walsh transforms. Hugh has taught communication theory and is a member of the IEEE. He recently left HP to work for a west coast company. He was born in Quincy, Massachusetts, is married, and has three children. He now lives in Palo Alto, California and enjoys outdoor activities and sports with his family.

33

Richard J. Conrad

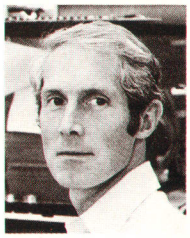

Jim Conrad was born in Hackensack, New Jersey and attended nearby Fairleigh Dickinson University, earning a BSEE degree in 1972. He continued his studies at Cornell University to earn a master's degree in electrical engineering in 1973. After working on a credit card transaction system for an east coast research lab for two years, he joined HP in 1975. Jim's 77200A Scanner design involved the front end and ultrasound image quality. His work has also resulted in one patent related to a physiological recording process. He has taught an introduction to microprocessors and served four years in the U.S. Navy. Married and the father of a son and a daughter, he lives in Hamilton, Massachusetts. His outside interests include skiing, bicycling, running, mountain climbing, and tennis.

Richard A. Snyder

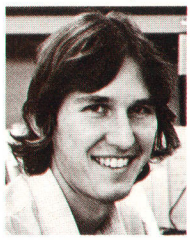

A graduate of Tufts University (BSEE, 1978 and MSEE, 1981), Rick Snyder came to HP in 1979 with experience in developing digital signal processors. He worked on the 77200A Scanner design and is now responsible for ultrasound image quality. Born in River Edge, New Jersey, he is single and lives in Chester, New Hampshire. His interests include mountaineering, bicycling, skiing, astronomy, and receiving weather satellite pictures.

39

Paul A. Magnin

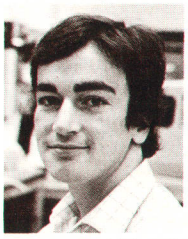

Paul Magnin's contributions have resulted in ten papers related to ultrasound imaging. With HP since 1981, he is manager of the image quality and ultrasonic tissue identification group at HP's Andover Division. Born in Marion, Indiana, he was educated at Princeton University (BSEE, 1977) and Duke University (PhD, 1981). He lives in Andover, Massachusetts.

A Physician's View of Echocardiographic Imaging

by Richard L. Popp, M.D.

A FEW PHYSICIANS ARE INTERESTED primarily in ultrasound, noninvasive imaging, or other applications of technology to medicine. But most physicians and health care professionals want medical information that will help them care for patients. This majority becomes interested in an imaging device if it provides new data not available by other means, more complete or more accurate data than competing methods, advantages such as obtaining data at less risk or less cost to the patient, or more convenience to the patient and/or physician. Ultrasound imaging is attractive because it can satisfy all these conditions.

One contribution of ultrasound imaging is the ability to "see" the heart or other structures inside the body without doing anything potentially dangerous to the patient. Another feature is the detail with which the anatomy of soft tissues, such as heart valves and heart walls, are displayed. Heart valves and walls move rapidly and no other widely available imaging method can show both structure and motion with such detail as two-dimensional ultrasound imaging (2-D echocardiography). Strictly speaking, I can't say that new conditions or diseases have been discovered by echocardiography, but this method has given us new information to help explain things we have only observed about patients in the past. For example, some patients develop heart failure after heart valve replacement surgery. Echocardiography is easily performed in the intensive care unit as well as in the laboratory and allows us to decide if the heart muscle or valve is malfunctioning. We can also tell if the heart is compressed by fluid accumulating within the chest or if the valve itself has pulled loose. In this example echocardiography is done rapidly and provides accurate information conveniently.

Clinical Use of Ultrasound Imaging

In general, echocardiography has made an important contribution to patient care because it is noninvasive (nothing need be injected into the body), it can be done without hospitalizing the patient (and so the cost is kept down), there is no ionizing radiation involved, and there is no known risk to the patient from performing the procedure. It offers improved differentiation of soft tissues which look the same in X-ray images and because of all of the above, it is quite repeatable. The repeatability translates to the ability to follow patients and learn the natural history of their condition with and without interventions to change that natural history. If the physician simply wants to make a diagnosis of a suspected condition, the physician might often use echocardiography now, whereas a cardiac catheterization, with attendant risk and cost, would have been the method of choice in the past. Certainly the echocardiogram is superior to any other technique for the diagnosis of small masses within the heart such as cardiac tumors and bacterial growths on the heart valves, and can better display fluid accumulations around the heart.

Making the statement that echocardiography is superior to other techniques has required a long process of testing. From a historical perspective one must realize that pulsed echo techniques date from the mid 1950s and high-volume use of echocardiography in the United States, and subsequently in the world, has evolved since approximately 1967. During the early part of this period, M-mode echocardiography was the only form available. This mode provides information on the dynamics of cardiac motion from only a single area of the heart at any given time since the ultrasound beam must be reoriented to encounter another part of the heart for study. The need to expand the display to provide an overall picture of the heart in anatomic format was appreciated, and 2-D echocardiography was invented in the early 1970s. This was quite rudimentary until the mid 1970s and the modern era of 2-D echocardiography has existed only the past five years or so. Although much of the data that is useful clinically is available through M-mode echocardiography for those who have learned how to interpret it, 2-D echocardiography makes the same data more comprehensible to more physicians and provides new data not available by M-mode.

Comparison of M-Mode and Two-Dimensional Methods

The extension of M-mode echocardiography to 2-D ultrasound imaging usually means increased cost. For this reason we must explore the relative value of the old and new methods. The high sampling frequency of M-mode (about 1 kHz) compared with 2-D echocardiographic images (about 30 Hz) means that very fast cardiac movements are tracked better with M-mode. For example, high-frequency vibrations of valve structures indicating abnormal flow are usually more obvious in M-mode than in 2-D images, and in fact may be imperceptible in 2-D studies. The subtleties of motion of individual echoes may be more easily analyzed by M-mode because 2-D images also seem to present information "overload" to the observer. That is, so much data is presented on a 2-D image that the observer may have trouble concentrating on a single echo among all of the signals making up the 2-D image. Very slight separations of the pericardial sac surrounding the heart seem more clearly defined, for example, using the limited sampling area of the M-mode technique. The human eye/brain combination has difficulty keeping track of both cardiac motion and the time base provided by the electrocardiogram. Thus, it may be easier to match events on the M-mode records when compared with 2-D images.

On the other hand, the expanded anatomic information presented by 2-D echocardiography has revolutionized the diagnosis of congenital heart disease, helping us to under-

stand the relative size of the heart chambers and the number of heart valves that are properly and improperly formed. The alteration in cardiac wall motion relative to more normal motion among segments of the heart is used to recognize and quantify the effects of coronary artery disease on the heart. This is done almost exclusively with 2-D echocardiography. The abnormal bulge (aneurysm) that is the result of heart attack in many patients is recognizable by 2-D methods and is not perceptible by most M-mode methods.

In fact, the combination of 2-D and M-mode methods often is optimal for understanding each type of record and best serves the patient. Because virtually all 2-D instruments are also capable of providing M-mode recordings, we need not pit M-mode against 2-D methods for diagnosis. It is more appropriate to compare the limited ability of M-mode methods alone versus the combination of 2-D images and M-mode recording for the comprehensive analysis of each case.

Although I have mentioned that current echocardiographic methods are extremely useful and that they are a relatively recent development, one may properly ask why physicians are not rushing out even more quickly to equip themselves with 2-D echocardiographic instruments? To answer this question we should first become familiar with the details of the information sought from the images created. With respect to the heart, the images may show abnormal structure such as a congenital malfunction, or distortion of the originally normal anatomy by disease processes such as rheumatic heart disease. The presence of structures that are not normally present, such as blood clots, tumors, or masses of bacteria within the heart, are seen and recognized as abnormal features (Fig. 1). The "better" the quality of the image produced by the instrument, the better our ability to recognize subtle abnormalities of structure, distortion of anatomy, or abnormal new structures. Anatomy also is important when one looks at the secondary effects of disease such as enlargement of heart chambers and altered shape of these chambers.

In addition to simply looking at the size and shape of the heart, the dynamic parameters of cardiac motion are of great interest to the cardiologist. Some abnormal patterns of motion alone represent disease processes such as those associated with rheumatic mitral valve disease. The amount the heart walls move tells us about the volume of blood moving through the heart and the rate of motion reflects the rate of volume change or flow. In addition to measuring the size and shape of the organ and observing the dynamics of the moving cardiac structures, one also can notice normal or abnormal appearance of the tissue being displayed. These alternations in tissue appearance, or tissue texture, are of special interest to the radiologist imaging abdominal organs, for example, but also are of great interest to the cardiologist. Currently we are able to recognize calcification of tissues such as the diseased aortic or mitral valve, scars that occur within the heart after heart attack, and infiltration of the heart with abnormal proteins such as amyloid. The ability to see all three types of information (anatomy, function, tissue integrity) is what determines a "good" system.

Equipment Considerations

Observing the size and shape of the heart, or other organs, means looking at measurements that depend on the resolution of the instrument. As resolution improves and the image becomes more clearly defined, it becomes easier for the user to outline the heart to measure its size and extrapolate this size to volume. A clear outline throughout the cardiac cycle leads to accuracy in measuring dynamic parameters. Differentiating very low-intensity signals from the background noise on the image is also important be-

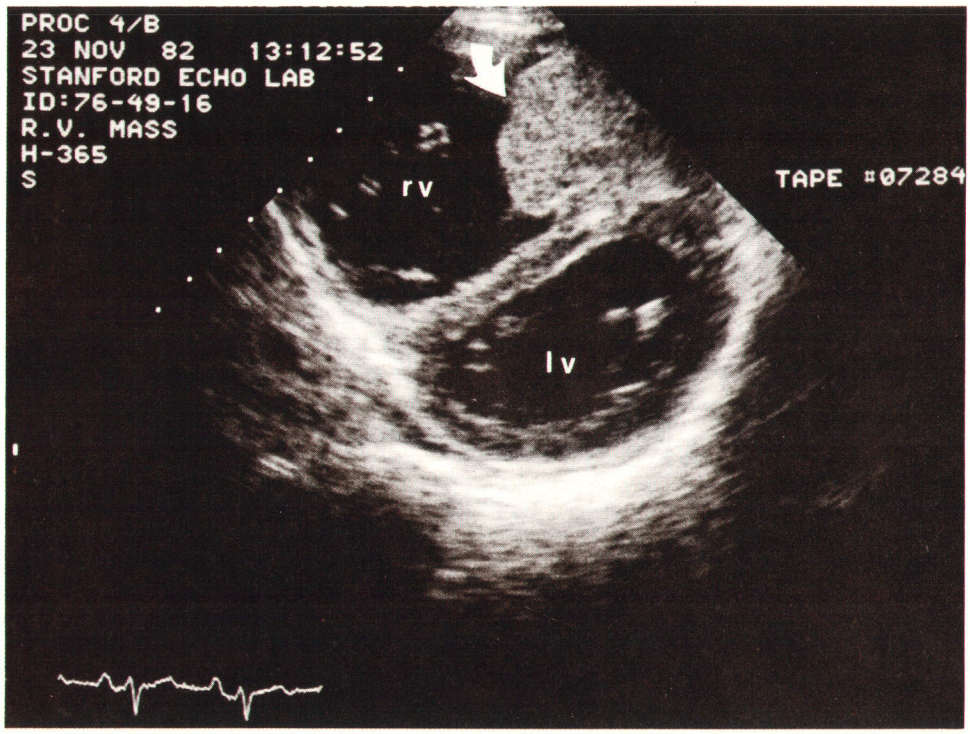

Fig. 1. *An echocardiographic image of the heart taken with the transducer on the chest wall in the parasternal position and oriented parallel to the short axis of the left ventricle (lv). The arrow indicates an abnormal mass within the right ventricle (rv) attached to the interventricular septum. The mass has visual features that make it appear different from the myocardium (heart muscle). The mass is a malignant tumor from a distant site which has traveled to and grown in the heart. Note the echo-free (black) ventricular chambers compared to the low amplitude echoes within the myocardium and the tumor. Wall thickness can be judged from this image even in the absence of specular echoes from the blood-muscle interface.*

cause it is the combination of very low-intensity and very high-intensity signals that produces the texture one uses to assess the quality of the tissue (Fig. 1).

As the various aspects of these considerations become optimized, ultrasound images become more and more similar to optical images of the organ being studied. Very clear pictures of the structures and lack of spurious instrument-generated echoes please the user (Fig. 2). Other features such as gray-scale mapping and processing schemes can alter the aesthetics of the picture, but these merely satisfy individual user preference, by and large. Optimizing the system also includes making it easy to use. This includes not only putting the minimum number of controls on the instrument, but also having these controls in the best possible location for use and making them easy to activate. Other considerations come from clinical use on hospitalized patients and these include the size of the transducer and the portability of the instrument.

More resolution is obtained by using a maximum aperture transducer, but the space between the ribs must be used for the sound entering the body and this means that a transducer face larger than 20 to 25 mm gives difficulty when applying it to the chest wall. The need to manipulate the transducer on the chest wall, tilting it and rotating it, produces special considerations for those designing the transducer case.

Finally, the acceptance of echocardiography has given rise to a need to use it to make clinical decisions on very ill patients, sometimes in life and death situations. As a result one often needs to transport the instrument to the intensive care unit, squeeze it between the patient's bed and the life support equipment, and rapidly record information in the midst of feverish activity around the patient. This requires a small, light, maneuverable, and easily used system with self-contained recording equipment.

The historical development of mechanical 2-D scanners and electronic phased-array 2-D scanners has led to some generalities about the equipment that is prevalent in the user public. The original advantage, the wide angle of view, of phased-array instruments over mechanical scanners is no longer present. The ability to record simultaneously M-mode data and 2-D images is mainly the property of phased-array scanners, although some mechanical instruments now have one transducer for 2-D imaging and a second transducer for simultaneous M-mode recording. Mechanical scanners are usually less expensive than phased-array scanners, although the gap is variable and narrowing. Mechanical scanners have a reputation for a less cluttered, low-background-noise image compared to phased-array devices. The phased-array systems originally had significant problems with spurious echoes contributed by grating lobes and generally had more complex controls. Phased-array instruments of the generation characterized by the HP 77020A generally are more sensitive when judged in the clinical sphere and compared with mechanical scanners. That is, the ability to get usable information on a very high percentage of patients seems better with these instruments than with most mechanical scanners. In general, the clean, clear images and "beautiful" pictures produced by the best mechanical scanners in patients that are easy to image have had a slight edge over the phased-array images for these patients. However, with even slight increases in imaging difficulty caused by biological and technical factors, the phased-array devices usually have been able to acquire clinically useful data when the mechanical scanners have not been up to the job.

General Thoughts on Echocardiographic Testing

To place the current application of echocardiography in proper perspective for its evaluation in the clinical setting, it is worthwhile to review the methods by which such applications are developed. With the invention of echocardiography, as well as the subsequent improvements culminating in the most advanced equipment, a general process applies. First, patients with well-confirmed or known disease are selected for testing with the new equipment to see the result. In this group of patients with 100% prevalence of the condition, the patterns of abnormality are defined and can be learned as examples of the "classic case." Assuming that there are characteristic abnormalities on the test accurately indicating a certain condition for the patients known to have the condition, then the method is applied to patients who are suspected of having the disease or process under discussion. In these patients the prevalence of the condition may be very low or very high, generally depending on the degree of rarity of the condition and also depending on the clinical acumen of the physician who has taken the history, done the physical examination, etc., before considering the new test.

For physicians to use echocardiography properly in various clinical settings, it is important to have data on the sensitivity and specificity of the test for the condition under discussion, to know the prevalence of the condition in the population, and to judge the probability of this individual patient having the condition sought. Learning to rely on the test when it is positive and/or negative requires a significant data base obtained from doing the test in patients with a well-defined presence or absence of the condition as validated by other accepted techniques. Such information is needed before we are able to say either that a condition truly is present when the test is positive, or that we can exclude the condition when the test is negative. If a physician is trying to confirm a strong clinical suspicion that the disease is present, then the physician wants a test that confirms the presence of disease when the test is positive or abnormal. Echocardiography does this extremely well. Conversely, if the clinician is trying to reduce the possible diagnoses in a given patient by progressively ruling out specific disease states, this process requires the clinician to exclude the disease confidently. In general one cannot exclude disease processes well with echocardiographic images. For example, when a large mass is present within the heart, we see it well. When we are trying to exclude the possibility of a mass, and none is demonstrated on the image, we are still left with the question whether there truly is no mass or whether it is so small that it is beyond the resolving capability of the instrument.

A related issue develops from application of echocardiography in some conditions where new information is uniquely available. For example, the presence of small masses, such as groups of bacteria on a heart valve, may be recognized with echocardiography when no other cur-

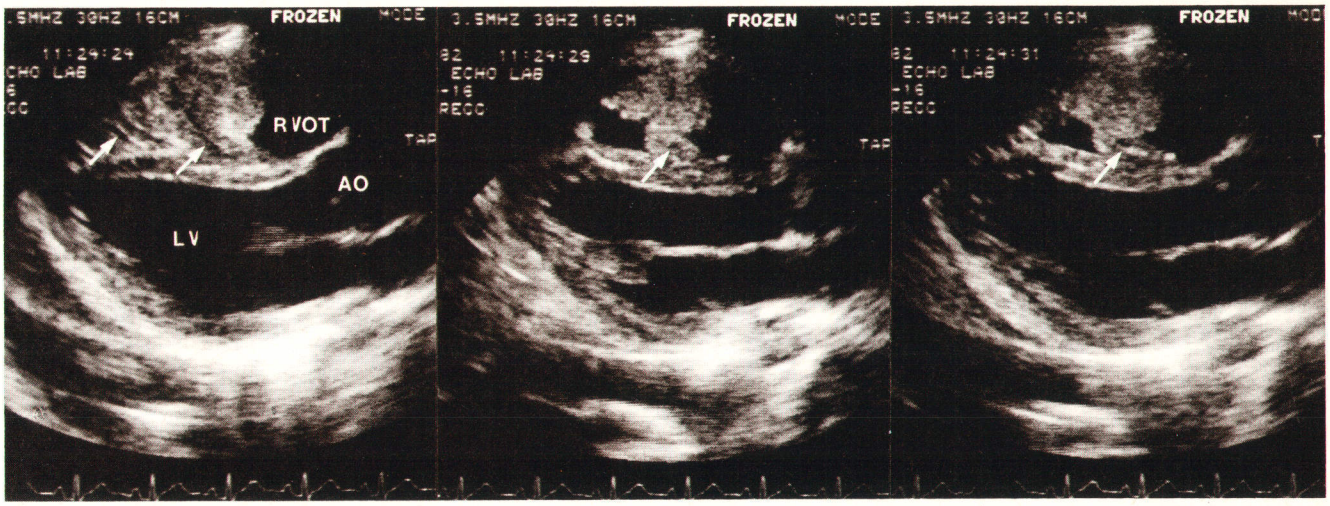

Fig. 2. *Three serial sections (images) parallel to the long axis of the left ventricle (LV) from the patient shown in Fig. 1. The mass within the right ventricle and right ventricular outflow tract (RVOT) contains very small blood vessels (arrows) that can be resolved with this imaging system. Serial sections of this type allow the echocardiographer to create a mental image of the spatial relations of the heart. (AO = aorta.)*

rently available technique can do this. If this new test is superior to the old test, then the new test seems valuable intuitively, but it is very difficult to prove this from a scientific standpoint. If bacteria are present in the patient's bloodstream and the echocardiogram does not show a mass within the heart, it is impossible to say whether this patient has an infection on the heart valve that is not shown by the echocardiogram, or whether in fact the bacteria in the bloodstream come from some other source within the body. This kind of consideration makes the establishment of sensitivity and specificity values for a new test very difficult.

We may consider using a relatively attractive noninvasive test in the screening of asymptomatic populations to look for disease processes. Again, depending on the prevalence within the population of the abnormalities sought, we can determine if using this test is worthwhile only when we know the sensitivity and specificity of the test for conditions we seek. Echocardiography possibly could be used for screening for some conditions, but at present the data base is not sufficient to help us determine whether this is worthwhile. We are in a phase of evolution in the technique and many of the expanded uses of the technique await data of this type. We can determine whether echocardiography is worth the cost only if we know both the quantitative accuracy of the method and when we know the impact of such information on long-term patient management. An example comes from using ultrasound imaging to help manage patients after heart attack. Most clinicians think they would like to know how much heart muscle remains, how well it contracts, and whether an aneurysm or abnormal scar is present after a heart attack. To get such information now, an angiogram or radionuclide study must be performed. If the patient can have echocardiography without radiation hazard and with reduced cost compared to these methods, and if the test is accurate, we can then design studies to learn if this information affects patient management and prognosis.

Training

The studies showing that echocardiography is very useful clinically and very accurate quantitatively have been done predominately by those with great skill and experience in the technique. Primary training in performance of echocardiography and interpretation of the results has been included in formal cardiology, radiology, and ultrasound training programs only within the past ten years. Recognition of the value of the method has created a tremendous need for training. Those people currently responsible for training people in echocardiography generally agree that a significant period of time is necessary to perfect the skills needed to perform the technique properly for clinical decision making. Guidelines have been established by the American Society of Echocardiography, and endorsed by other organizations, for both physician and technician training in both M-mode and 2-D echocardiography.

Between three and six months of physician training and experience is needed for independent interpretation of M-mode and 2-D echocardiography. This time commitment makes training quite difficult for the practitioner who may not be able to suspend a medical practice. Several proposals are now under consideration for dealing with this problem, but lack of proper training opportunities means echocardiography may be performed suboptimally in some settings and patients who would benefit from its optimal use may be denied this clinically important method.

An Acoustic Transducer Array for Medical Imaging—Part I

by John D. Larson III

THE ACOUSTIC TRANSDUCER ARRAY is the analog front end of an ultrasound imaging system. It provides a large number of independent channels, transduces electric signals to acoustic pressure, and generates sufficient acoustic energy to illuminate the various structures in the human body. In turn, it converts the weak returning acoustic echoes to a set of electric signals which can be processed into an image. The key transducer requirements are to:

- Generate 10 to 100 mW/cm^2 of acoustic power from reasonable input voltages
- Provide good signal-to-noise ratio
- Have low cross-coupling between elements
- Generate short acoustic pulses, ≈2 μs in duration
- Couple acoustic energy to the patient efficiently
- Damp the acoustic backwave
- Achieve broad angular coverage
- Suppress undesired vibration modes
- Be lightweight and handheld.

Although a variety of techniques for generating and detecting sound are available, piezoelectric transducers are preferable because they can both generate and receive acoustic waves, and they are several orders of magnitude more sensitive than other possible transducers.[1]

To construct an array from typical ceramic piezoelectric materials, a number of fabrication and performance problems must be solved. This article discusses the fabrication of a transducer array for medical imaging and some of the basic principles and design constraints that must be considered. The following article on page 22 describes the application of these considerations to the design of the transducers for the HP 77020A Ultrasound Imaging System.

Coupling to Patient and Short Pulse Generation

A pulsed 2.5-MHz piezoelectric transducer with no matching or damping layers rings and produces a long pulse on the order of 10 μs or more. Because range resolution is inversely proportional to pulse length, this resonance is unacceptable. Placing the transducer in contact with the patient neither damps this resonance greatly nor couples energy very efficiently because there is more than a 20:1 acoustic mismatch between currently available piezoelectric materials and the human body.

To obtain a shorter pulse that is more effectively coupled to the patient, several techniques can be used singly or in combination. The goal is to reduce the 20-to-30-dB insertion loss caused by the large impedance mismatch and to produce pulses short enough to allow 1-mm range resolution.

Ceramic Resonator in Direct Patient Contact. The loaded quality factor Q_L of a ceramic resonator in contact with a mismatched impedance (Fig. 1a) and possessing its own internal mechanical Q, Q_m, is given by:[2]

$$Q_L = \pi \frac{1+r^2A}{1-r^2A}$$

where $A = \exp(-2\pi/Q_m)$ and r is the reflection coefficient.

For a typical lead-zirconate-titanate (PZT) ceramic, $r = 0.88$, $Q_m = 70$, and Q_L is 18.4. The time response is a damped sinusoid of the form

$$\exp(-\pi f_o t/Q_L)\ \sin(2\pi f_o t)$$

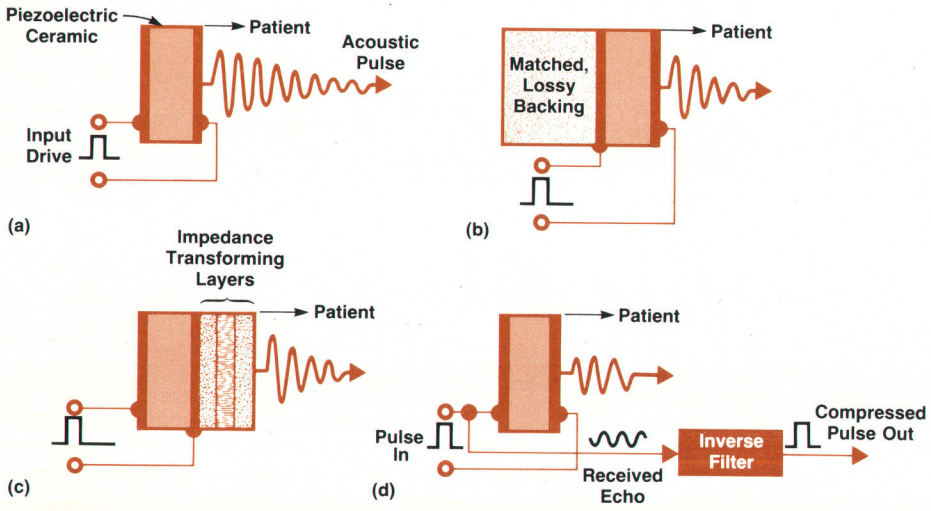

Fig. 1. *Schemes to obtain short pulses of ultrasound from acoustic transducers. (a) Undamped piezoelectric transducer placed directly on the patient. (b) Approach of (a) with backside damping added. (c) Using acoustic-impedance-matching layers to improve coupling between the patient and the transducer. (d) Approach of (a) using transversal filter processing to compress received pulse.*

For a resonator with $f_o = 2.5$ MHz, it takes 8.1 μs for the response to drop 30 dB, and the resulting range resolution (6 mm) is unacceptable.

Matched, Lossy Backing. If an acoustically matched and absorbent backing is added to the rear of the transducer (Fig. 1b), the effective Q_L is lowered to ≈ 2 and the pulse length is reduced to ≈ 1 μs. The acoustic energy propagated into the backing, or backwave, is lost by acoustic attenuation and no secondary resonances are set up. For example, for lead metaniobate ceramic material operating at 2.5 MHz and transmitting ultrasound into human tissue, the pulse duration is 1.3 μs. The insertion loss, including transduction efficiency and the impedance mismatch of ceramic to tissue is -28 dB.

This technique clearly improves the pulse response, although most of the power (>99%) is lost in the backing. It also has the advantage of minimizing the number of acoustic bonds and acoustic parts.

Matching Layers Between Transducer and Patient. In this realization (Fig. 1c), one or more matching layers are used to improve the transmission of acoustic energy into the body. The effective Q_L of the resonator is reduced, so a shorter pulse of ultrasound can be obtained. For example, a typical PZT ceramic with two matching layers of appropriate acoustic impedances interposed between the ceramic and the patient has a -4-dB insertion loss and a 2.1-μs pulse duration. This represents a large improvement in transduction efficiency with some loss of pulse length compared to the case shown in Fig. 1b.

Inverse Filter. As mentioned earlier, the pulse excitation of an unbacked transducer (Fig. 1d) yields a damped sinusoidal waveform. A compression filter might be built that takes a sinusoidal waveform and yields a pulse output. One such realization is an inverse filter.[3] In principle, substantial pulse compression can be obtained. In practice, the finite noise in the received signal limits the filtering process and the compression is limited to reduction factors of 2 to 3 in pulse length.[4]

The techniques illustrated in Fig. 1b and Fig. 1c are used in the 77020A Ultrasound Imaging System because of good pulse response and decreased insertion loss. These attributes lead to lower drive voltages, higher reception sensitivity, and pulse lengths commensurate with the desired range resolution.

Packaging Requirements and Constraints

A basic requirement of a phased-array transducer is that the elements be placed on half-wavelength ($\lambda/2$) centers to sample the aperture properly. Here λ is measured in the subject material. For the 1.5-to-2.5-cm apertures used for medical imaging, 60 to 80 elements are required. In turn, the ceramic transducer must be a half-wavelength ($\Lambda/2$) thick to operate properly. Here Λ is measured in the ceramic. Thus, the elements have a width-to-thickness ratio directly proportional to the velocity of sound in the piezoelectric ceramic and inversely proportional to the velocity in tissue. This ratio is about 3:1, resulting in tall narrow elements.

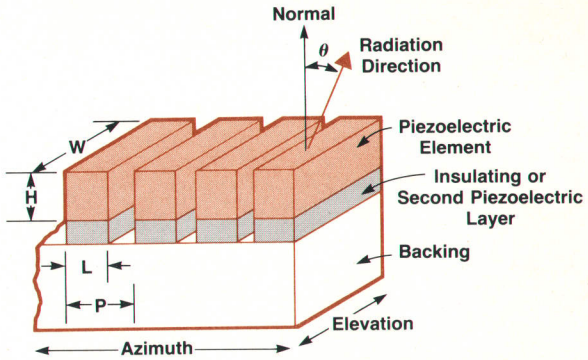

Fig. 3. *Basic acoustic transducer array configuration.*

Fig. 2 illustrates the possible lead connection schemes. An independent lead to each element is required. In Fig. 2a, the high-voltage electrodes ($\approx$200V pulse present) are toward the patient, causing a safety hazard. To overcome this, the high-voltage electrodes can be located on the backing side of the element if the backing material is an insulator (Fig. 2b).

The preferred structure is illustrated in Fig. 2c. Here an insulator is placed between the backing and the ceramic. A metal foil is bonded over the elements to form the ground connection, protect the patient, and keep grease out of the kerfs between elements (the elements are cut apart to suppress cross-coupling).

An important modification is to use a second layer of piezoelectric ceramic as the insulating layer. This gives suppression of the unwanted mass-spring mode and increases the acoustic energy radiated by the transducer.

Array Element Design

The acoustic arrays used in the 77020A's handheld transducers are composed of a large number of identical elements. These elements must be protected from the outside world of grease and dirt, and must be packaged with a suitable lens and case to provide a useful probe.

Driving Point Considerations. Each array element appears electrically to be a frequency-dependent, lossy capacitor with capacitance $C_o = \epsilon_s WL/H$ where ϵ_s is the clamped dielectric constant and W, H, and L are defined in Fig. 3. As will be seen later, these dimensions are constrained by

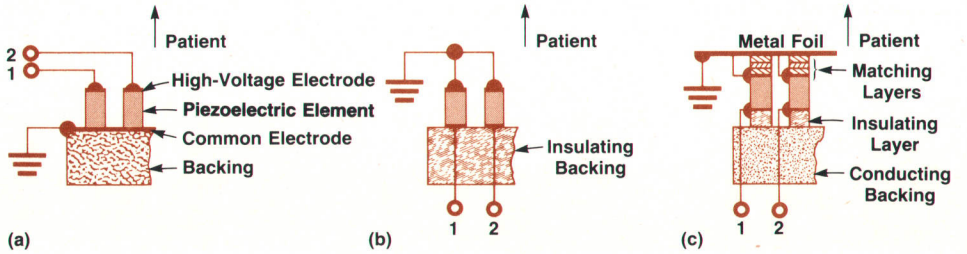

Fig. 2. *Possible electrode configurations for acoustic transducer arrays. (a) High-voltage electrodes toward patient, conducting or insulating backing. (b) Grounded electrodes toward patient, insulating backing. (c) Grounded electrodes toward patient, conducting backing.*

the need to control spurious modes and grating lobes, and to obtain a narrow beam in the elevation direction.

A compromise between high-frequency, shallow-penetration operation on one hand and low-frequency, deep-penetration operation on the other leads to choosing a center frequency of 2.5 MHz, a frequency which is assumed in the examples to follow.

To satisfy the above conditions, the dimensions L = 250 μm, period P = 320 μm, W = 10 mm, and H = 600 μm for PZT-5H ceramic material were chosen, and C_o = 55 pF.

Transmit Considerations. Exposure of mammalian tissue to average power densities of 100 mW/cm^2 or less has been found to cause no significant biological effects.[5,6] The design goal has been to stay below this power level. Detailed calculations show that for PZT-5H, a single-layer array element can achieve 100 mW/cm^2 for a 200:1 duty cycle with 216 volts peak-to-peak drive. A double-layer element develops the same acoustic power output at 130 volts peak-to-peak. The use of acoustic matching layers can allow more efficient power generation. For example, a single matching layer used in conjunction with a single PZT layer could result in a transduction efficiency increase of 8 dB, or around 90 volts peak-to-peak to achieve 100 mW/cm^2.

Another piezoelectric material of interest is lead metaniobate. It is similar to PZT-5H, but its dielectric constant is only one-sixth as great and it has a lower electroacoustic coupling coefficient. Its chief attraction is a low spurious mode level. For a 200:1 duty cycle and 100 mW/cm^2 power level, a single lead metaniobate layer requires 540 volts peak-to-peak drive while a double layer requires 360 volts peak-to-peak. The high drive voltage makes it less suitable for use with solid-state circuitry.

Since the acoustic arrays are operated in a pulsed mode to achieve good range resolution, wideband operation becomes a prime consideration. Factors influencing this include frequency-sensitive driving-point impedance, epoxy bond thickness, and frequency-dependent transduction efficiency. Other vibration modes can cause narrowband,

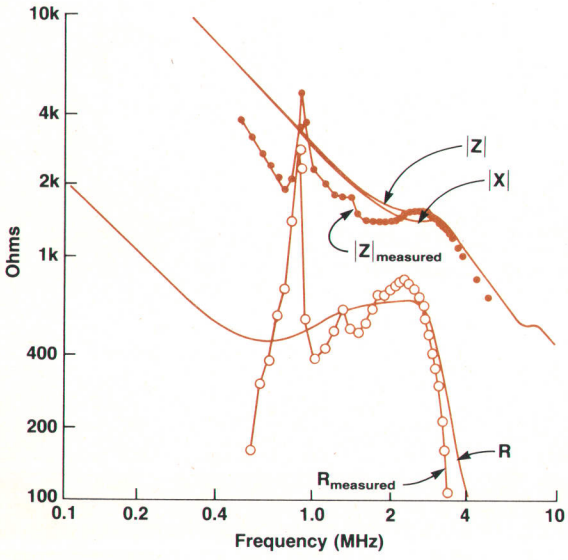

Fig. 4. *Input impedance versus frequency for a single PZT-5H element.*

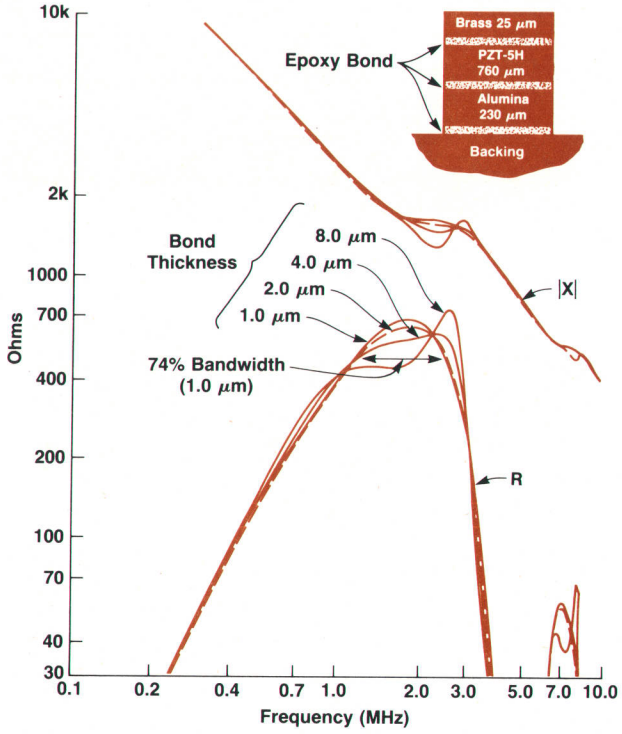

Fig. 5. *Effect of epoxy-bond thickness on the components |X| and R of the input impedance Z = R + j|X|.*

extended-time-duration response.

Using a circuit model for an acoustic transducer, the driving-point impedance of a single-layer PZT array element can be calculated as given in Fig. 4. The magnitude decreases with increasing frequency while the real part reaches a peak around the 2.5-MHz center frequency. Furthermore, by comparing measured data to the theoretical data, it is apparent that there are high-Q modes of vibration present which the simple circuit model does not predict.

Epoxy Bond Effects. The transducer response is quite dependent on the quality of the acoustic properties of the bonded array. Chief among these are the thicknesses of the epoxy-bond layers used to cement the PZT to the backing, the surface layers present on the backing, and the degree to which the backing impedance is the same as the PZT acoustic impedance.

The epoxy bond has an acoustic impedance of 3.2×10^6 rayls, compared to 25×10^6 rayls for PZT-5H. This 8:1 mismatch dictates that the bond be very thin to prevent narrowing of the passband. Fig. 5 shows how the frequency response of the transducer is changed as the bonds vary from 1 μm thick to 8 μm thick. In turn, the bandwidth varies from 74% to 31% as this occurs. To ensure good response, bond thicknesses less than 2 μm are required.

Acoustic Modes of Narrow Elements. In an acoustic imaging array the elements should have a single mode of vibration, namely a piston-like motion of the front surface. By making the elements sufficiently narrow, and reducing cross-coupling, the acoustic intensity should be uniform at various angles from the normal (see Fig. 3), that is, omnidirectional. For illumination out to angles where the re-

sponse is no more than 3 dB down from that at normal incidence, the element width L should be $\leq 0.44\lambda/\sin\theta_{3dB}$ which for ±45° coverage and 2.5-MHz operation, yields $L_{max} \leq 320\ \mu m$.

Fabrication constraints force the actual elements to be even narrower. With the element thickness H comparable to L_{max}, additional modes can be expected to exist at frequencies near the desired thickness mode frequency. Such vibrations include the dilatational or breathing mode, the mass-spring oscillation mode, Lamb wave on a foil, and the Rayleigh surface-wave mode.

Onoe and Tiersten[7] give a good account of the thickness and dilatation modes. Defining a configuration ratio G = L/H, it can be shown that these modes are close in frequency and strongly coupled when G = 1. For G << 1, the modes become widely separated in frequency.

Fig. 6 illustrates these two modes for 760-μm-thick PZT-5H at G = 0.1 to 1.3. The thickness mode frequency is essentially constant at 2 MHz while the dilatational mode frequency is inversely proportional to width L.

Another major acoustic vibration mode is termed the low-frequency mode[8] because of its manifestation at frequencies around 0.8 to 1 MHz, as compared to the main thickness mode at 2 MHz. It occurs as a fairly high-Q, slowly damped resonance which requires 40 to 50 μs to decay below the system noise level. The origin of the mode appears to be a harmonic oscillation of the element moving against the spring formed by the backing material. The frequency of this mass-spring mode can be given by $f_{m\text{-}s} = v_{eff}\sqrt{1/LH}$, where $v_{eff} = \sqrt{c_b/\rho_{PZT}}$, c_b is the elastic constant of the backing, and ρ_{PZT} is the density of the piezoelectric element.

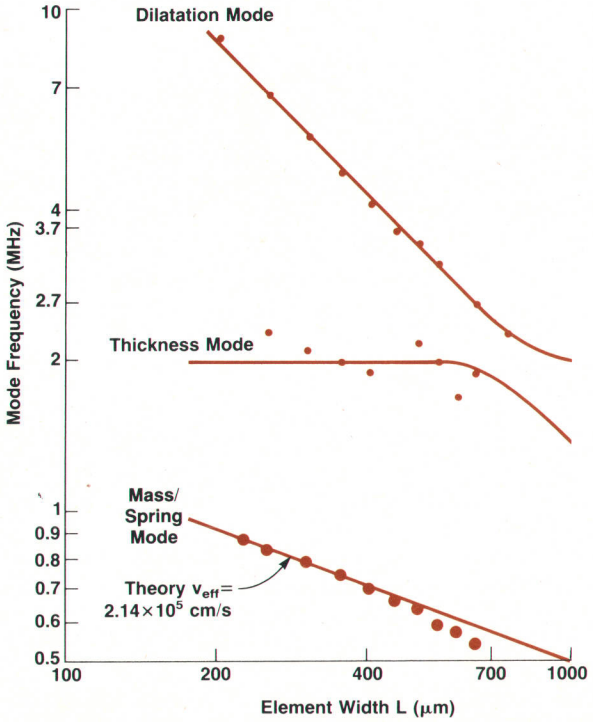

Fig. 6. *Mode frequency for the principal modes versus element width L for an element height H = 760 μm. (The dots indicate measured values.)*

The main effect of the mass-spring mode on transducer performance in an acoustic imaging situation is to add clutter to the image for the range from 0 to 7 cm because the mode is highly excited by the transmit drive pulse.

A thin metal foil is bonded to the top surface of the array to seal the element interstices. This foil can support a guided wave known as the Lamb wave.[9] Two subgroups can be identified depending on particle motion of the foil. The symmetric modes show particle motion where both sides of the foil move away from each other or towards each other. They are relatively nondispersive, that is, the acoustic velocity does not vary greatly with frequency. The asymmetric modes exhibit flexural propagation with velocities approaching zero as the frequency or plate thickness goes to zero. In metal foils, the symmetric mode has a velocity of about 4×10^5 cm/s, while the asymmetric mode varies from 0 to 2×10^5 cm/s. The excitation of these modes comes from the motion of a driving element, and is manifested mainly by cross-coupling between elements.

The last major mode that exists on the array is a Rayleigh surface wave.[10] This propagates on the backing with velocities in the range of 1 to 2×10^5 cm/s. The particle motion is a retrograde ellipse composed of components along the surface and perpendicular to it. This motion decays exponentially with depth from the surface. This mode is driven by the motion of an element and is another cause of cross-coupling between elements.

Mode Suppression. Of the modes discussed, the thickness mode is desired and all others are undesired. The dilatational mode is not suppressed, but by choosing narrow elements, the mode is moved to a higher frequency where it is conveniently filtered out.

Of the remaining modes, the mass-spring mode is most troublesome. It is strongly excited and has high Q. Its occurrence around 1 MHz is inconveniently close to 2.5 MHz in terms of filtering. In one scheme, this mode is suppressed by using two oppositely poled pieces of PZT to cause a zero net center-of-mass motion. This results in an order of magnitude reduction of the mode as measured by the real part of the input impedance. Shorter ring-down times, less cross-coupling, and more uniform acoustic radiation patterns result.

The Lamb wave is suppressed by choosing a very thin foil. Since the asymmetric mode is largely responsible for Lamb-wave propagation, making the foil thin reduces the group velocity and prevents effective coupling from the array elements to the foil.

Since the Rayleigh wave is bound to within a few wavelengths of the backing surface, making deep cuts extending well into the backing effectively suppresses it.

Element Angular Response. The angular response of a compensated single element is shown in Fig. 7. This measurement was made by sending a signal to a point reflector at angle θ from the normal to the transducer and then recording the return voltage. For such a round-trip or in/out type measurement, the normalized signal $s(\theta)$ depends on frequency and element width as $s(\theta) = 20\log((\sin x/x)\cos\theta)$ where $x = (\omega L/2v)\sin\theta$, ω = radian frequency, and v = acoustic velocity in water. The main points to note are that the element response drops off because of the finite element

width L and the obliquity factor $\cos\theta$.

Lens. The acoustic beam generated by the one-dimensional phased array described here can only be electronically focused and steered in the azimuth plane (see Fig. 3). To improve the resolution and sensitivity further, a cylindrical acoustic lens[11,12] is added to give a fixed focus in the orthogonal elevation plane.

The main properties of interest in a lens are the resolution at focus, radius of curvature to achieve a given focus, the depth of field about that focus, and the intensity gain caused by focusing. The lens must be sufficiently strongly focusing to achieve better resolution than an unfocused beam, yet have enough depth of field to allow imaging over a useful range. This involves a compromise in the elevation aperture W. In addition, reverberations caused by a poor lens impedance match to the patient are to be avoided. Finally, low attenuation in the lens and a convex outer surface are important considerations.

The desired focal length F is related to the lens radius of curvature R by $R = F(1 - 1/n)\gamma_l$ where $\gamma_l = 1.4$ (empirically determined for the acoustic lens material used), $n = v_1/v_2$, v_1 = acoustic velocity in the lens, and v_2 = acoustic velocity in the patient.

The elevation beamwidth D_y at F is given by $D_y = \lambda(F/W)$ where λ = acoustic wavelength in the patient. The depth of focus $D_z = 15D_y(1 - 0.01W/2F)$.

Array Fabrication

Referring again to Fig. 3, the fabrication of an array probe involves the following processes, materials, or steps.

- Synthesis of a highly attenuative backing material with close impedance match to PZT
- Cutting, polishing, and plating the various ceramic materials and matching layers
- Bonding the array together with sufficiently thin bonds
- Dicing the elements
- Providing electrical connections to the closely spaced elements
- Applying a top ground foil electrode
- Synthesizing and attaching a suitable lens
- Packaging the array into a probe complete with cable and connectors.

The backing is required to match PZT acoustically and have sufficiently high acoustic loss to damp any backwave to a level below the system noise. Typically a 50-to-60-dB round-trip loss at any signal frequency above 1 MHz is required. If the loss is not large enough, multiple echos will return and cause bright lines or "range markers" in the image. The backing material chosen is a composite of tungsten for high impedance and polyvinyl chloride (PVC) plastic as a binder and dissipative medium. Typical parameters achieved are an acoustic impedance of 25×10^6 rayls, a density of 14.2×10^3 kg/m^3, and an attenuation of 20 dB/cm at 1 MHz. Typically the attenuation increases as frequency squared, so at 2 MHz the loss is 80 dB/cm.

The raw PZT-5H material used for each element is wafered to the appropriate dimensions, then ground and polished to a final thickness of 600 to 700 μm. The thickness and the parallelism of the sides are carefully controlled.The parts are poled by a high electric field in a heated oil bath to make them piezoelectrically active.

The backing and ceramic parts are very carefully cleaned under dust-free conditions, then bonded together with low-viscosity epoxy resin. Matching layers are also bonded at this stage, as is the electrical lead structure. To avoid the various cross-coupling problems outlined earlier, the 64 individual elements are separated by sawing.

The array is thoroughly cleaned again and a thin metal foil is bonded on to complete the ground connection and isolate the array elements from infiltration by grease, coupling gel, or water.

A variety of acoustic lenses can be used. A convex single-element lens is an effective choice, but the selection of useful materials is limited to those in which the acoustic velocity is less than that in human tissue (1.54×10^3 m/s). The lens material used for 77020A transducers is a polyurethane rubber, Sylgard 170®. It provides a good impedance match to human tissue and the acoustic velocity in Sylgard 170 is 1.02×10^3 m/s. This allows the design of a convex lens with a radius $R = -36$ mm for a 7-cm elevation focal length. It is fabricated on a thin foil by casting and then is bonded to the array.

The final array is wired to a suitable coaxial cable containing 64 individual leads. It is then packaged in a waterproof plastic case. Fig. 1 on page 22 shows a photograph of a completed unit.

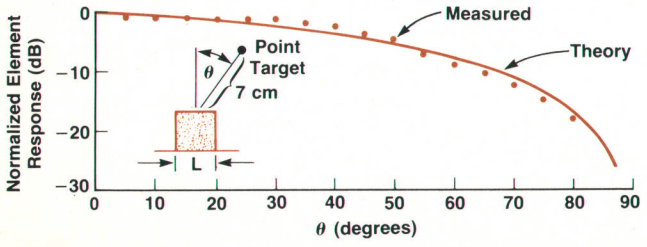

Fig. 7. *Round-trip response (received echo from a point target) versus azimuth angle for a single acoustic element.*

Acknowledgments

Many people at HP Laboratories have been part of this effort. George Nelson, Johnny Ratcliff, and Henry Yoshida have contributed greatly to all the technical phases of piezoelectric ceramic preparation, fabrication, and wiring the finished unit.

David Wilson did the early lens design work. Fleming Dias contributed to broadbanding the transducer response. Amin Hanafy helped with the Lamb-wave suppression studies.

References

1. K.Y. Wang, "A High-Sensitivity Ultrasonic System for Real-Time Diagnosis," *1974 IEEE Ultrasonics Symposium Proceedings*, pp. 753-755.
2. M.T. Wauk II, *Attenuation in Microwave Acoustic Transducers and Resonators*, PhD Dissertation, Stanford University, July 1969, pp. 101-102.
3. G.L. Kerber, R.M. White, and J.R. Wright, "Surface-Wave Inverse Filter for Non-Destructive Testing," *1976 IEEE Ultrasonics Symposium Proceedings*, pp. 577-581.
4. Y. Murakami, et al, "An Application of Weiner Filtering to Non-Destructive Evaluation," *Applied Physics Letters*, Vol. 33,

no. 8, October 15, 1978, pp. 685-687.
5. G. Kossoff, "On the Measurement and Specification of Acoustic Output Generated by Pulsed Ultrasonic Diagnostic Equipment," *Journal of Clinical Ultrasound*, Vol. 6, no. 5, October 1978, pp. 303-309.
6. Notice of Intent to Propose Rules for Diagnostic Ultrasound, *Federal Register* 44, no. 31, Tuesday, February 15, 1979.
7. M. Onoe and H.F. Tiersten, "Resonant Frequencies of Finite Piezoelectric Ceramic Vibrators with High Electromechanical Coupling," *IEEE Transactions on Sonics and Ultrasonics*, July 1963, pp. 32-39.
8. J.D. Larson, "A New Vibration Mode in Tall, Narrow Piezoelectric Elements," *1979 IEEE Ultrasonics Symposium Proceedings*, pp. 108-113.
9. T.N. Grigsby and E.J. Tajchman, "Properties of Lamb Waves Relevant to the Ultrasonic Inspection of Thin Plates," *IRE Transactions on Ultrasonics*, March 1961, pp. 26-33.
10. I.A. Viktorov, *Rayleigh and Lamb Waves*, Plenum Press, New York, 1967, Chapter 1.
11. P.N.T. Wells, *Biomedical Ultrasonics*, Academic Press, New York, pp. 36-42.
12. T. Tarnoczy, "Sound Focusing Lenses and Waveguides," *Ultrasonics*, July-September 1965, pp. 115-127.

An Acoustic Transducer Array for Medical Imaging—Part II

by David G. Miller

HIGH SENSITIVITY and a short pulse are important, but conflicting requirements for an acoustic transducer used in diagnostic imaging systems. The design of the transducer (Fig. 1) for the HP 77020A Ultrasound Imaging System is a compromise between these two requirements. Optimizing this compromise required careful consideration of the physical parameters and design constraints discussed in the preceding article (page 17).

Acoustic Pulse Propagation

Lead zirconate titanate, a ferroelectric ceramic crystal, was chosen for the 64 piezoelectric elements in the transducer array because of its high electromechanical coupling and high dielectric constant. The piezoelectric behavior occurs as a result of either a zirconium or titanium ion locating in a stable off-center position inside the otherwise symmetrical lead and oxygen unit crystal cell (see Fig. 2). Because this ion has a large charge, this creates noncoincidental centers of negative and positive charge in the unit cell, forming an electric dipole.

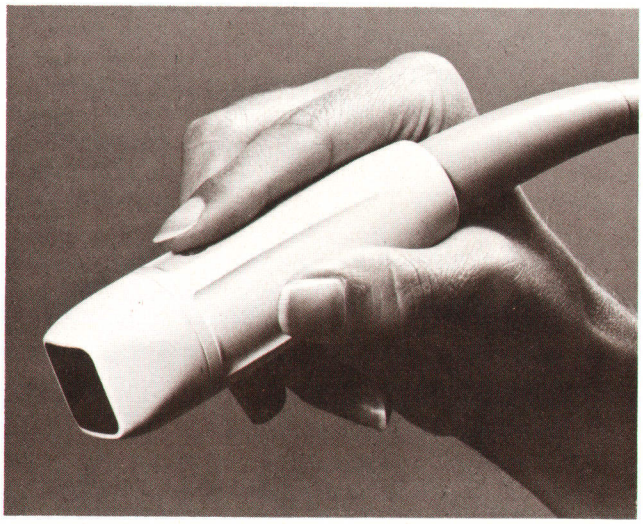

Fig. 1. *One of the ultrasonic transducer probes used by the HP 77020A Ultrasound Imaging System.*

Polarizing the material orients a majority of these dipoles in the same direction. This is done by applying an external electric field to crystals heated above their Curie temperature and then cooling the crystals. This process, called poling, uses the property that above the Curie temperature, the unit cell is a body-centered cubic structure (Fig. 2a). As the crystal cools, the ion in the center of the structure moves off center in a direction influenced by the applied electric field. After the crystal is cooled to room temperature and the electric field is removed, the ions stay in their off-center locations to form the polarized crystal.

If a voltage is applied to opposite faces of a polarized crystal, a field is produced in the crystal that acts upon the dipoles to cause expansion and contraction of the crystal. By applying an alternating voltage, acoustic waves are propagated from the stress discontinuities occurring at each face of the crystal as it expands and contracts.

Each element of the 64-element transducer array is a 0.5-mm-thick slab of lead zirconate titanate polarized in the plane of the slab and having electrodes on each end as shown in Fig. 2c on page 18. Compression and rarefaction longitudinal waves are propagated in both the forward and reverse directions. Waves traveling in the reverse direction are absorbed by the transducer's backing to prevent echoes

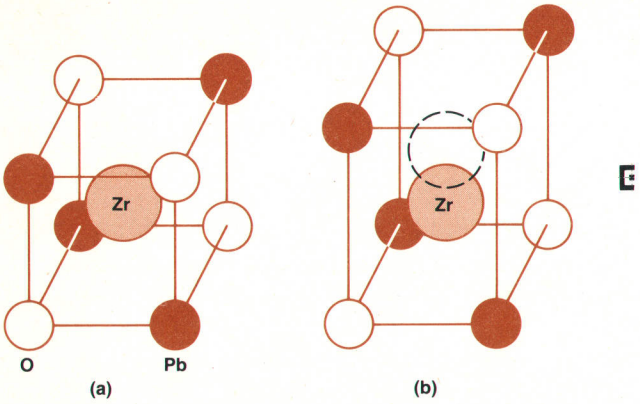

Fig. 2. *The lead zirconate titanate crystal unit cell is a body-centered cubic structure (a) above the Curie temperature. Below the Curie temperature, the zirconium ion moves off center to form a tetragonal structure (b).*

from objects behind the transducer. This backing also helps damp the multiple reflections occurring inside each element. Waves radiating from such a transducer are represented in Fig. 3.

The acoustic impedance of the transducer elements is about 25 times greater than that of the human body. A sevenfold increase in the magnitude of the acoustic echo from a target in the body can be achieved by reducing the impedance mismatch between the transducer elements and the body. This is done by placing an intermediate impedance-matching layer between the elements and the body. To prevent reverberation inside this layer and maximize the magnitude of the acoustic wave, the matching layer is made a quarter wavelength thick at the transducer's center frequency.*

*Quarter-wavelength matching was first used by early astronomers who discovered that faint stars were brighter when viewed with telescopes that had old tarnished lenses rather than new untarnished ones. The tarnish layer turned out to be about a quarter wavelength thick and have an intermediate index of refraction between that of the glass and the air. In modern times, coating optical components with quarter-wavelength-thick layers has become commonplace and interest in quarter-wavelength impedance matching of electrical transmissions lines has resulted in an extensive development of the theory.

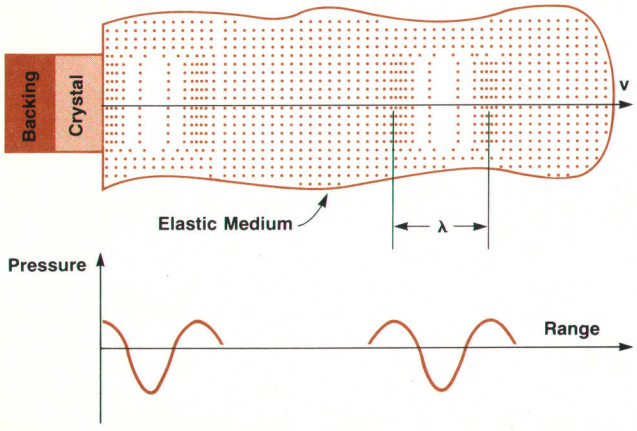

Fig. 3. *Longitudinal compression and rarefaction waves traveling to the right with velocity v for an acoustic transducer radiating pulses of wavelength λ. Particles along the axis of propagation oscillate to the right and left.*

The constructive interference produced by the quarter-wavelength matching layer is illustrated in Fig. 4. The acoustic wave pulse is represented as a ray r which strikes the layer at normal incidence (shown at a slight angle to show the reflection r_1 within the layer) and emerges as the sum of rays r and r_1. The magnitude and phase of r_1 may be determined from the reflection coefficient

$$R = \frac{Z_2 - Z_1}{Z_2 + Z_1} \quad (1)$$

Thus a 180° phase change occurs for reflected waves when a pulse propagates from a high-impedance (Z_1) region to a low-impedance (Z_2) region. And it follows that since the reflected ray r_1 travels an extra distance of one half wavelength within the intermediate matching layer, this 180° phase change aligns r_1 to be in phase with r so that the original pulse and reflected pulse amplitudes add as shown in Fig. 4.

Equivalent Circuit Model

To select the optimum acoustic impedance for the intermediate matching layer and try to account for the effects of the electrode metallization and other features of the transducer array construction, an equivalent circuit model was developed. The KLM model [2] of an acoustic transducer is an electromechanical equivalent circuit (Fig. 5) in which the transducer is excited at the center. The acoustic load impedances can be transformed to the center node by the transmission line equation

$$Z_{IN} = Z_o \frac{Z_L \cos(\pi d/\lambda) + jZ_o \sin(\pi d/\lambda)}{Z_o \cos(\pi d/\lambda) + jZ_L \sin(\pi d/\lambda)} \quad (2)$$

The circuit regards force (stress times area) as equivalent to voltage, and acoustic wave velocity as equivalent to current.

Consider what happens when the front and back terminations are not perfect. The waves produced at the center suffer reflections at the faces, giving rise to a total stress and velocity that depend on the reflection coefficients at each surface. The stress, and hence the voltage V, will tend to be maximum when both the incident and reflected waves are strong. This occurs near resonance; therefore, the transducer should be a half wavelength long for strongest excitation. If at resonance the crystal is a half wavelength long and each transmission line becomes a quarter wavelength long, Equation (2) simplifies to

$$Z_{IN} = Z_o^2/Z_L \quad (3)$$

However, reflections from both surfaces tend to make the transducer ring, producing an output pulse like a decaying sinusoidal waveform whose decay rate depends on both the acoustic impedance mismatch and the electrical loading of the transducer.

Denoting the transformed front and back load impedances by Z_{FO} and Z_{BO}, the circuit can be redrawn as shown in Fig. 6. Hence, the fraction of the power radiated to the body is

$$P_F = \frac{V^2/Z_{FO}}{V^2/Z_{BO} + V^2/Z_{FO}} = \frac{Z_F}{Z_B + Z_F}$$

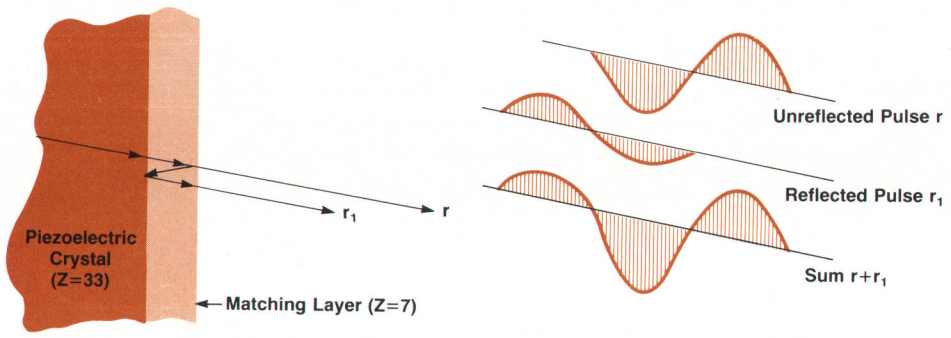

Fig. 4. *Illustration of constructive interference in a quarter-wavelength-thick matching layer. The normal rays r and r_1 are drawn at a slight angle to their true direction so they can both be seen.*

and the conflict between high sensitivity and a short pulse is apparent. High sensitivity requires a low backing impedance Z_B, but the shortest pulse requires matching the front and back acoustic loads to the crystal to reduce ringing.

Matching the front of the crystal is further complicated because the crystal has an acoustic impedance Z_o of 33×10^6 rayls and a body's acoustic impedance is only 1.5×10^6 rayls. Thus, the power percentage radiated to the body by a transducer with a matched backing and unmatched front is only 4%.

The effects of the quarter-wavelength matching layer discussed earlier can be modeled by adding another transmission line to the front port of the KLM model.[3] This layer acts as a mechanical transformer, causing a large load to be reflected to the transducer. With this matching layer, the radiated power percentage at resonance increases from 4% to 27% and the same improvement occurs in receiving the acoustic echo. By using Equation (3), the acoustic impedance required for the matching layer can be calculated from

$$Z_{IN} = Z_o = Z^2_{layer}/Z_{body}$$

Transducer Test System Design

by George A. Fisher

Early in the design of the phased-array transducer for the 77020A, the need for accurate acoustic measurements was realized. As new designs were investigated, accurate and repeatable measurements of the acoustic beam profile, main beam rolloff, pulse length, ring down, and overall array sensitivity were especially important because these factors are critical to the overall performance of a phased-array imaging system. Measurements of individual element sensitivity and electrical impedance as a function of frequency provide additional information about acoustic beam performance. Individual element capacitance measurements provide a quick go/no-go check of array integrity for manufacturing and physical shock survival experiments.

To perform this wide variety of measurements easily, a special test system is required. It must be flexible so that new experiments can be added easily as different areas of transducer performance are evaluated. It is also desired that the system be easy to use so that measurements can be made by lab technicians instead of engineers. Finally, because of the huge range of signal levels resulting from echoes from various targets in the body, the total dynamic range of the system should be at least 80 dB.

To meet the above performance specifications, a test system (Fig. 1) was designed around an HP 9825A Computer. With proper I/O expansion, this provides flexibility for new experiments as well as the intelligence required to provide ease of use and measurement accuracy. For mechanical accuracy, a special mechanical stage was designed to hold and position the array accurately in a tank of water along with a variety of test target reflectors and transducers. The system also uses a regular production 77020A Ultrasound Imaging System scanner to control the firing and receiving of the array signals. A few custom hardware components were added to provide an interface to the scanner and tank positioning system. A flexible disc drive was added for program and data storage, and a plotter is used as the principal output device for analytical measurements. For impedance and capacitance measurements, a network analyzer and an LCR meter are interfaced to the 9825A.

The mechanical stage holds the transducer securely in position, facing downward into a tank of water, which closely approximates the acoustic impedance of the body. The virtual central axis of the transducer is manually aligned with the axis of an adjustable arm that swings through an arc of ±50° under control of the 9825A. The arm can be adjusted to position the target reflector at various depths of interest. The stage holding the transducer is also controlled by the 9825A and can be pivoted in the elevation direction. These movements allow positioning the target and transducer in azimuth and elevation directions for measuring beam directivity and focus.

The 9825A Computer is the heart of the system. It provides convenient control of many variables during tests, as well as a simple operator interface. In addition, it enhances the accuracy of the system by performing calibration routines and then saving correction data.

Another function performed by the 9825A is that of extending the dynamic range of the system. The gain of the ultrasound scanner used to transmit and receive the acoustic beam is controlled by the 9825A by means of a digital-to-analog converter (DAC), which feeds the TGC (time gain compensation) inputs of the scanner. The gain of the scanner can be varied by 60 dB. Before tests are performed, the 9825A feeds a test signal through the scanner and measures the scanner's gain as a function of TGC voltage. This data is saved on a flexible disc. During actual tests, the 9825A controls the TGC voltages to the scanner in such a manner as to maintain the widely varying received signal in the middle of the available dynamic range of the scanner, and

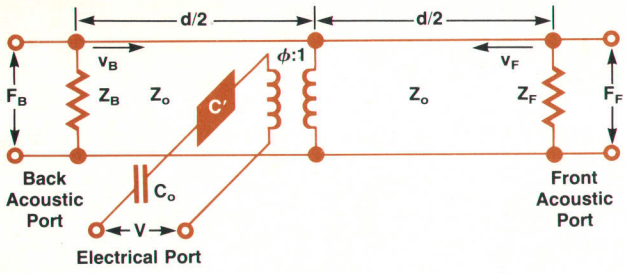

Fig. 5. *Model of piezoelectric transducer after Krimholtz, Leedom, and Matthaei.[2] Here A is the cross-sectional area of the element, d is its length, ϵ_s is the clamped dielectric constant, and $C_o = A\epsilon_s/d$ is the clamped capacitance. C' represents the acoustic energy storage, ϕ is the ratio of induced acoustic velocity (equivalent current) to the electrical current, Z_o is the characteristic acoustic impedance of the crystal, ω_o is the half-wavelength frequency of the crystal, v_F and v_B are stiffened acoustic velocities, and Z_F and Z_B are the front and back acoustic load impedances.*

which yields a layer impedance of 7.0×10^6 rayls.

Lens Design

The performance of the transducer is also determined by the shape of the acoustic beam in both the direction of the scan and normal to the scan (elevation). An acoustic lens was designed for the elevation focusing.

The minimum angular beamwidth for a focal point placed anywhere in the range is given by the diffraction limit $\theta = \lambda/W$, where λ is the acoustic wavelength and W is the aperture.[4] The geometric focal length of a lens can be derived by a geometric construction based upon Fermat's Principle* and the same approximation that produces the lens maker's equations for optical lenses.[5] Thus, for a thin plane convex lens,

$$\text{Focal length} = \frac{\text{Radius of lens surface}}{(v_{body}/v_{lens}) - 1}$$

*Fermat's Principle states that a light ray will take the path between two points that requires the least travel time.

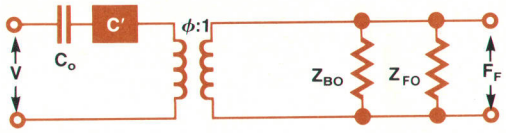

Fig. 6. *Simplified equivalent circuit using transformed load impedances.*

corrects the measurements by the stored gain values. This gives the system a total dynamic range considerably greater than 80 dB.

For measurements of both overall and individual element sensitivity, the 9825A communicates with the scanner via the HP-IB (IEEE 488), putting the scanner into a special test mode that allows the computer to take over control of transmit firing and receive phasing. The computer fires just two elements in the center of the array, which results in nearly omnidirectional acoustic radiation. This is reflected by a small target. The computer also controls the scanner so that the signal from only one element at a time is processed and measured. This allows the sensitivity of each individual element to be measured.

The electric impedance and capacitance of each element are measured with the network analyzer and LCR meter. Each instrument is connected to one transducer element at a time through a programmed relay matrix. This matrix contributes stray capacitance and inductance to the measurements, so before tests are run, the 9825A measures these stray values by performing tests on known impedances, calculating the errors, and storing these values. For impedance measurements, the computer controls the measurement frequency with a DAC connected to the FM input of the network analyzer. At each frequency, and for each element in the array, the computer relates the measured impedance of the element to its actual impedance via a two-port network calculation using the stored data.

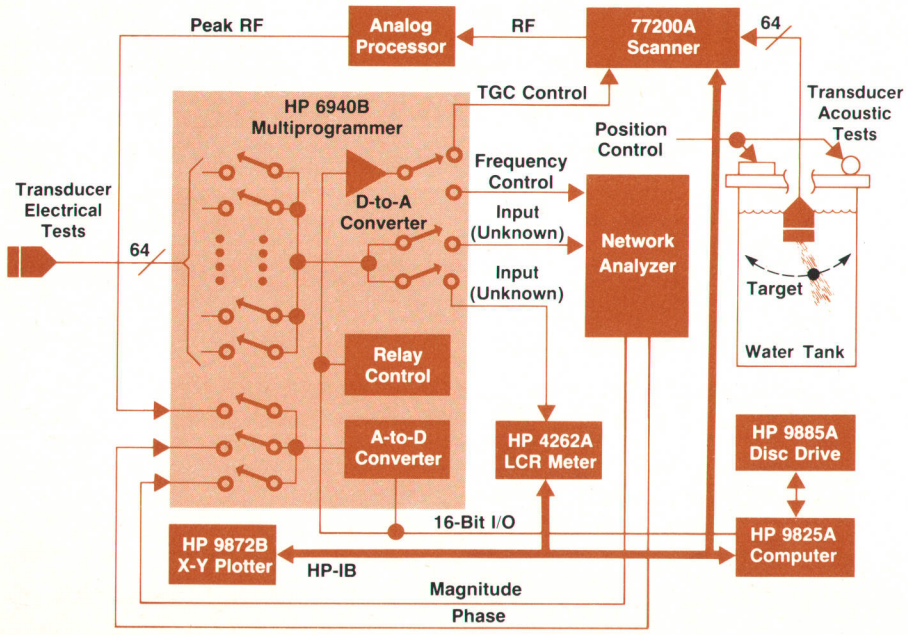

Fig. 1. *Block diagram of transducer test system.*

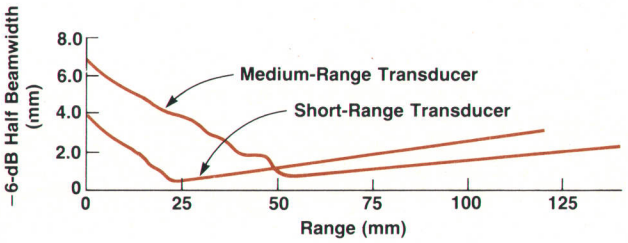

Fig. 7. *Calculated round-trip beamwidths for 3.5-MHz, fixed-focus, short-range and medium-range transducers.*

where acoustic velocities v_{body} and v_{lens} are used directly in place of the refractive indexes used in conventional optics.

But geometric optics theory gives very poor beamwidth predictions because the apertures are relatively small—10 to 20 acoustic wavelengths. These small apertures produce beams dominated by diffraction effects and are not well described by converging and diverging rays. Another complication is the pulsed operation rather than the continuous-wave operation for which the diffraction equation is valid.

The optimum aperture and focal length combination produces the minimum beamwidth through the range of interest. Two different combinations are illustrated in Fig. 7. The short-range transducer has a short focal length lens and a small aperture to reduce the beamwidth near the transducer. The medium-range transducer uses a larger aperture to reduce the beamwidth at midrange.

The acoustic lens design also requires the selection of a material with the proper acoustic velocity and impedance to match the human body. Velocities lower than that in the body allow a convex face on a flat transducer array. Velocities higher than in the body require a concave lens surface or the use of two lens elements. Other lens requirements are low attenuation for all beam steering angles, resistance to abrasion, chemical resistance to acoustic coupling gels, cleaning disinfectants, and sterilization, and providing a permanent seal to the transducer package. A convex lens is used for the 77020A's transducers.

Acknowledgments

Many people contributed to the ultrasonic transducer array development. Those at HP Laboratories are cited in the preceding article. At HP's Andover Division, the project team included James Chen, Jim Fearnside, Amin Hanafy, Dan Latina, Jerry Leach, Gary Seavey, Tom Stephens, and Tom Szabo. We are grateful for the skills and ideas provided in prototype construction by Maureen Bouchard and Joni Comeau, among many others.

References

1. L.H. VanVlack, *Elements of Material Science*, Addison-Wesley, Reading, Massachusetts, 1966.
2. D.A. Leedom, R. Krimholz, and G.L. Matthaei, "Equivalent Circuits for Transducers Having Arbitrary Even-or-Odd Symmetry Piezoelectric Excitation," *IEEE Transactions on Sonics and Ultrasonics*, Vol SU-18, no. 3, July 1971.
3. C.S. Desilets, J.O. Fraser, and G.S. Kino, "Design of Efficient Broadband Piezoelectric Transducers," *IEEE Transactions on Sonics and Ultrasonics*, Vol. SU-25, no. 3, May 1978, pp. 115-125.
4. J.W. Goodman, *Introduction to Fourier Optics*, McGraw-Hill, New York, 1968.
5. D. Haliday and R. Resnick, *Physics*, John Wiley & Sons, New York, 1962.

Radiated Power Characteristics of Diagnostic Ultrasound Transducers

by Thomas L. Szabo and Gary A. Seavey

WHAT LEVELS OF ULTRASONIC POWER are safe? This is an often asked question to which there is still no absolute answer, but some guidelines have been developed. People working with diagnostic imaging and other uses of ultrasound in medicine have established safe levels of ultrasonic intensity below which no bioeffects have been demonstrated. Ulrich[1] developed a threshold based on a compilation of biological effects data. He arrived at a criterion for minimal hazard: a spatial-average, temporal-average intensity below 100 mW/cm^2. This criterion and others have been used to summarize the lowest levels at which bioeffects have been observed. For example, see Fig. 1 adapted from Nyborg.[2] All of these observations can be summarized by the following statements:

- No substantial bioeffects have been demonstrated for spatial-peak, temporal-average intensities <100 mW/cm^2.
- No substantial bioeffects have been demonstrated for exposures for which the product (I×t) is less than 50

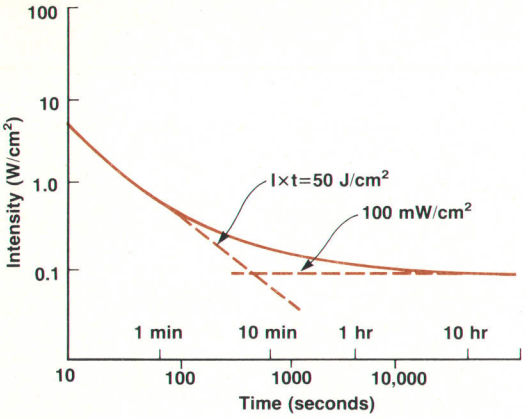

Fig. 1. *Suggested safe ultrasound intensity levels based on the lowest levels at which biological effects have been reported in tissues (adapted from reference 2).*

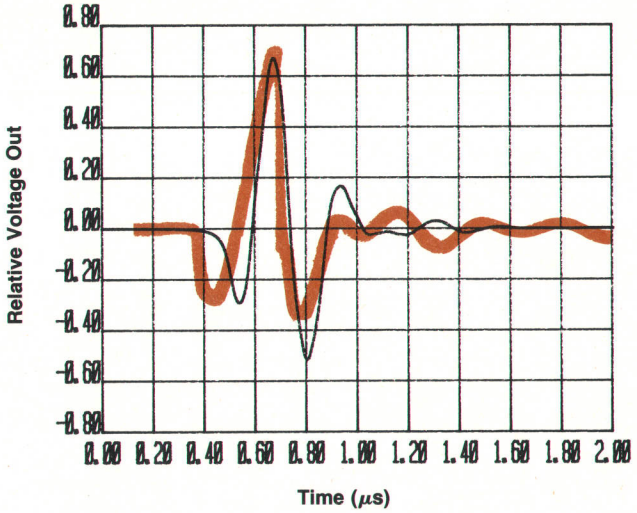

Fig. 2. *Measured and computer simulated temporal pressure waveforms at the spatial peak for the HP 21205B Transducer.*

J/cm^2, where for pulsed operation, t is total on-and-off time, and I is the spatial-peak, temporal-average intensity.

These results are incorporated in the "Safety Standard for Diagnostic Ultrasound Equipment."[3] Definitions and measurement recommendations outlined in the standard are used by the HP Medical Group for characterization of ultrasound transducers and systems. Before explaining these measurement techniques, it is necessary to answer the question: "How does a transducer provide a certain level of acoustic intensity in the body?"

Transducers

A transducer serves two main functions: converting electrical drive signals into acoustic waves, and directing and focusing these waves in the body. The transducer also receives acoustic echoes from the body that are used to form the ultrasound image, but the emphasis here will be on the transducer as a transmitter.

Although the HP 21205B 3.5-MHz Transducer (see Fig. 1 on page 22) appears externally as one transducer, it is actually a phased array of 64 transducer elements. Each element has a certain electroacoustic conversion transducer efficiency TE′ when connected to a continuous-wave (CW) voltage generator V_g with an impedance R_g. In terms of acoustic peak power P_a at the face of the element, $TE' = P_a/P_g$, where $P_g = V_g^2/4R_g$ is the generator power.

A transducer can be thought of as a bandpass filter with a certain impulse response. To find the temporal-average acoustic output, the input waveform also must be considered. Most diagnostic imaging transducers are driven by short pulses repeated at long time intervals. A common drive pulse is a tone burst of n half cycles, each t_o in length. The shape of the input pulse determines the temporal-average power per pulse. For a tone burst, this power is $P_g/2$. The average power is half as large as the peak power, so an average power factor apf can be defined in this case as apf = 0.5. Another important factor in reducing total average power is the duty cycle, which is the drive pulse duration t_p divided by the pulse repetition interval T_R. In the HP 77020A Ultrasound Imaging System, the duty cycle is typically 0.0005. Fig. 2 compares a computer simulation of one acoustic temporal pressure output waveform of a single 3.5-MHz element in water with an actual waveform.

The temporal-average acoustic power of all of the elements at their faces can be calculated using the equation:

$$P_{avg} = N(TE)(P_g apf)(t_p/T_R) \quad (1)$$

where TE is now defined as the temporal-average acoustic output divided by the average electrical input power for the drive pulse used.

Beamforming

To improve image definition, the transducer array directs and focuses acoustic energy by two methods. With reference to Fig. 3, the beamforming can be separated into orthogonal elevation and azimuth planes. In the elevation plane perpendicular to the transducer element widths, a fixed lens covers the array and focuses the beam. At the focal

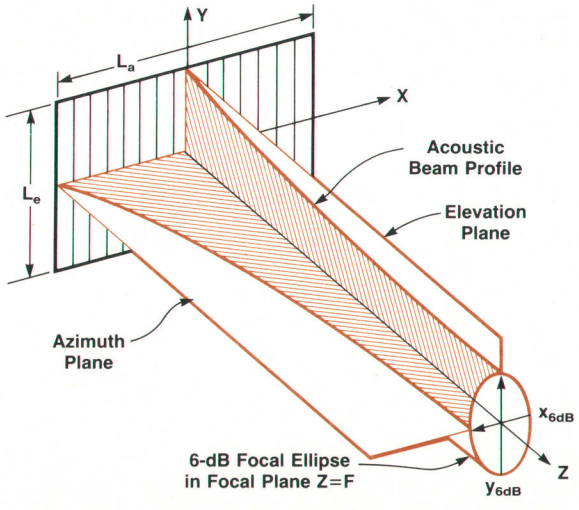

Fig. 3. *Definition of acoustic beam profiles in azimuth and elevation planes.*

plane Z=F, the beam shape for an elevation aperture L_e is the Fourier transform of the constant-amplitude aperture function $\sin(\pi L_e x/F\lambda)/(\pi L_e x/F\lambda)$. A simple estimate of this large compression of the beam is the half-amplitude (6-dB) half beamwidth.

$$x_{6dB} = 1.9F\lambda/\pi L_e \quad (2)$$

where λ is the acoustic wavelength in water.

In the azimuth plane, focusing and beam steering are accomplished by addressing each phased-array element with appropriately phased, time-delayed signals. As shown in Fig. 3, the beam is focused in azimuth along the Z axis at the same place as the elevation focus. The Z axis constitutes one line in the ultrasound image (0° line); other lines are formed by directing the beam to other angles in the azimuth plane. At the focal plane, a 6-dB or quarter-power ellipse can be defined with half beamwidths (Equation (2)) for semiaxes. If the spatial-average, temporal-average intensity I_{SATA} is defined at the focal plane as the average power in the integrated beam cross section divided by the area of this ellipse, the following formula applies to the ideal example discussed.

$$I_{SATA} = 0.9P_{avg}/L_eL_a \quad (3)$$

where L_a is the total azimuth aperture. When the intensity at the peak is measured by a microprobe transducer and time averaged, the value is referred to as the spatial-peak, temporal-average intensity I_{SPTA}.

Another commonly quoted intensity is the spatial-peak, pulse-average intensity I_{SPPA}. This single-pulse intensity is the temporal average without the duty cycle t_p/T_R. Therefore, $I_{SPPA}=I_{SPTA}(T_R/t_p)$ as evident from Equation (1).

To compare actual measurements with predicted values, a measurement scheme, outlined in reference 3, is used. This method uses a hydrophone probe, its calibration, and integration algorithms for spatial and temporal averaging.

Transducer Hydrophone

To characterize the radiated acoustic power both spatially and temporally in absolute power terms, a special calibrated miniature hydrophone is used. This hydrophone has a piezoelectric element approximately 1 to 2 mm in diameter fabricated of polyvinylidene fluoride (PVF_2) film.

Since acoustic intensity is proportional to the pressure squared, and the hydrophone output voltage V is proportional to pressure, a hydrophone sensitivity can be defined as $K = I/V^2$, where I is the instantaneous intensity and V is the instantaneous voltage response of the hydrophone.

An X-cut quartz transducer calibrated by the U.S. National Bureau of Standards is used as the reference power source to determine the hydrophone's sensitivity. The radiated acoustic power P_t versus transducer drive voltage V_g has been measured using a force balance to arrive at a radiation conductance G_r, where $P_t=G_rV_g^2$. The hydrophone is positioned in the far field on the beam axis of the quartz transducer. The hydrophone's response V(0,t) to the radiated temporal pressure is recorded. A number of radial scans are taken to characterize the spatial distribution of the radiated pressure. Since the total radiated acoustic

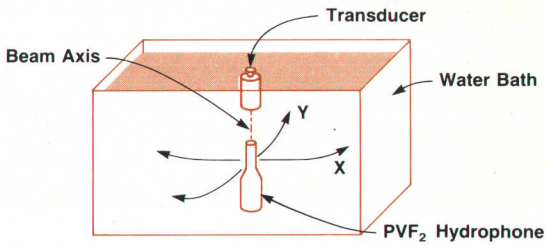

Fig. 4. *Acoustic intensity measurement apparatus.*

power from the quartz transducer is known from $P_t=G_rV_g^2$, knowing the temporal and spatial characteristics of the radiated pressure, one can do a temporal and spatial average of the pressure squared to relate the hydrophone's sensitivity to the measurement taken. This intensity response factor K for a given frequency is

$$K = \frac{P_t V_p^2(0)}{h\,b} \quad (4)$$

where P_t is the total radiated acoustic power in watts from the source transducer into the water, $V_p(0)$ is the temporal-peak hydrophone response on the beam axis, and h is the temporal average of the hydrophone response on the beam axis. That is,

$$h = \frac{1}{T_R}\int_0^{T_R} V^2(0,t)\,dt \quad (5)$$

where V(0,t) is the hydrophone response waveform. Here b is the spatial normalization computed from the spatial scan measurements. For rectangular transducers,

$$b = \int_{-x_{6dB}}^{x_{6dB}} \int_{-y_{6dB}}^{y_{6dB}} V_p(x,0)V_p(0,y)dx\,dy \quad (6)$$

where $V_p(x,0)$ and $V_p(0,y)$ are temporal-peak hydrophone responses along orthogonal beam profiles through the beam axis, and x_{6dB} and y_{6dB} are the 6-dB half beamwidths.

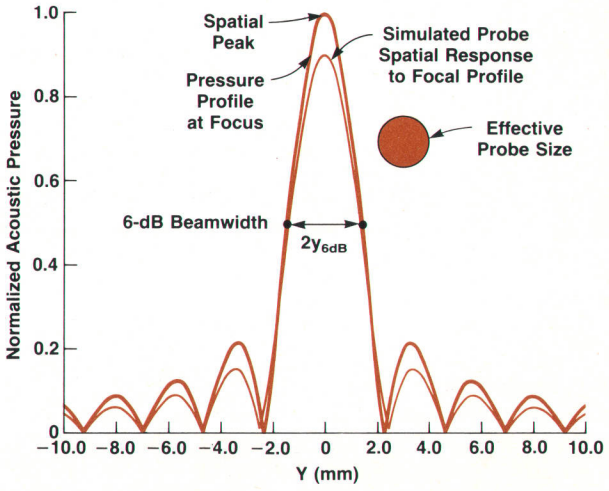

Fig. 5. *Acoustic pressure profile or beamplot at the focal plane of a transducer compared to a probe measurement simulation.*

Measurements and Definitions

To characterize the radiated acoustic power from an ultrasound imaging system, one must be able to find the most intense part of the transducer beam in three dimensions and measure the acoustic pressure waveform there. A sketch of the water tank arrangement used to make these measurements is shown in Fig. 4. The support structure (not shown) allows accurate alignment of the transducer and hydrophone and automated positioning of the calibrated hydrophone.

When the hydrophone is positioned on the beam axis at the spatial peak, the calibrated hydrophone temporal output waveform V(0,t) is recorded. A typical waveform is shown in Fig. 2 and it agrees well in shape with the predicted pressure waveform for a single element. The measured waveform is squared and integrated over a long period T_R to determine I_{SPTA} using the following equation.

$$I_{SPTA} = \frac{K}{T_R}\int_0^{T_R} V^2(0,t)\,dt \qquad (7)$$

To find the spatial average of the intensity, more detailed information about the beam is gathered. To do this, only the temporal value V_p is used from each waveform for these spatial measurements. Next, the hydrophone is scanned along two orthogonal paths within the spatial-peak plane to map the pressure profiles, $V_p(x,0)$ and $V_p(0,y)$.

A typical spatial pressure profile such as $V_p(0,y)$ appears similar to the ideal pressure beam profile in Fig. 5. At the 6-dB points in each pressure profile, a half beamwidth is determined. These half beamwidths, x_{6dB} and y_{6dB}, like the ideal of Equation (2), determine the measured focal ellipse depicted in Fig. 3. This ellipse has an area $A = \pi x_{6dB} y_{6dB}$. The final value of I_{SATA} is given by

$$I_{SATA} = \frac{I_{SPTA}}{A}\,\frac{b}{V_p^2(0,0)} \qquad (8)$$

This equation is based on measurable values and its result can be compared to the ideal estimate given by Equation (3).

Conclusions

At this time, safe levels for diagnostic ultrasound systems are those agreed on by consensus. Carefully worded definitions insure that those who make intensity measurements are speaking the same language. Results for different types of diagnostic systems are listed in Table I. HP systems fall in the range of an automatic sector scanner in this table.

HP transducer arrays and ultrasound systems are evaluated according to the methods described above. Transducer modeling and beamplot computer programs, along with equations such as Equations (1) and (3), have been used to predict acoustic intensity levels with good accuracy. Hence, the mechanisms that produce acoustic intensities are well understood and can be changed by design.

Work is also continuing on refining the measurement process itself. In Fig. 5 the effective hydrophone probe diameter is shown in relation to a typical pressure profile. Because the beam is comparable in size to the probe diameter, the probe smooths or integrates the actual pressure profile. The estimated hydrophone response is the second curve in Fig. 5. Because the hydrophone probe was calibrated originally against a quartz source much larger than its diameter, its calibration factor K is strictly applicable only in similar environments. The effect shown in Fig. 5 is that a slight error of about 1 dB is introduced at the spatial peak. Other sources of error are under investigation to improve the measurement accuracy further.

References

1. W.D. Ulrich, "Ultrasonic Dosage for Nontherapeutic Use on Human Beings: Extrapolations from a Literature Survey," *IEEE Transactions on Biomedical Engineering*, Vol. BME-21, 1974, pp. 48-51.
2. W.L. Nyborg, "Physical Mechanism for Biological Effects of Ultrasound," *HEW Publication (FDA) 78-8067*, U.S. Government Printing Office, Washington, D.C., 1978
3. "Safety Standard for Diagnostic Ultrasound Equipment," *AIUM/NEMA Standards Publication No. UL1-1981*.

Table I

Intensity Ranges Produced by Current Ultrasound Systems

Type of Equipment	Spatial-Average, Temporal-Average Intensity on the Radiating Surface	Spatial-Peak, Temporal-Average Intensity	Spatial-Peak, Pulse-Average Intensity
Static Pulse Echo Scanners and M-Mode Equipment	0.4-20 mW/cm²	10-200 mW/cm²	0.5-280 W/cm²
Automatic Sector Scanners (Phased Arrays and Wobblers)	2.7-60 mW/cm²	45-200 mW/cm²**	25-100 W/cm²
Sequenced Linear Arrays	0.06-10 mW/cm²	0.1-12 mW/cm²	25-100 W/cm²
Pulsed Doppler, Primarily for Cardiac Work	3-32 mW/cm²	50-290 mW/cm²	3-14 W/cm²
Doppler Instruments, Primarily for Obstetric Applications	3-25 mW/cm²	Spatial Peak Intensity: 9-75 mW/cm²	
CW Doppler, Primarily for Peripheral Vascular Applications	38-840 mW/cm²	Spatial Peak Intensity: 110-2500 mW/cm²*	

* Estimate based on the spatial average—temporal average.
** This value was measured with the scanning mechanism arrested for M-mode and at the maximum system pulse repetition rate.

A Scan Conversion Algorithm for Displaying Ultrasound Images

by Steven C. Leavitt, Barry F. Hunt, and Hugh G. Larsen

IN THE HP 77020A Ultrasound Imaging System, the signals received by the 64 acoustic transducer elements and processed by the electronic scanner correspond to the return echoes from an acoustic beam focused in a direction that changes with time in a predetermined manner. The digital scan converter in this system processes this information to present a visual image of the acoustically scanned region. This converter uses a novel two-dimensional interpolation algorithm in a process referred to as R-Theta reconstruction. Using this technique, the acoustic image is reproduced from the echo values in an essentially error-free manner.

Review of Acoustic Data Processing

After the 64 individual signals received by the transducer array are appropriately phased, delayed, and summed, the result is a single waveform consisting of bursts of sinusoidal activity. This activity is a fairly broadband set of pulses at frequencies near the transducer's resonant frequency. Spatially, this waveform corresponds to the echoes along a narrow line directed radially outward from the center of the transducer's face. A total of 121 such acoustic rays are used to form a 90° sector image (Fig. 1). The waveform for each ray is routed to a full-wave rectifier, a peak detector, and a low-pass filter to extract the modulation envelope. The envelope is sampled, first at 15 MHz, and then at a slower rate dependent on the selected scan depth. This allows the use of a fixed number (396) of sample points per ray to represent different scan depths of 4, 8, 12, 16, 20, and 24 cm. The array of 121×396 five-bit samples is sent from the 77020A's scanner to the digital scan converter for image formatting.

Hence, the data received by the digital scan converter is the result of a two-dimensional sampling process. Not only is the data sampled radially, it is sampled laterally in the angular or azimuth dimension. All of the concepts relevant to the Shannon sampling theorem associated with a time-based waveform (the radial sampling) apply equally well to spatial sampling.The implication is that, given samples from a two-dimensional sampling process, and if the sampling frequencies are sufficiently high, then in principle, the image may be reconstructed without error from these samples.

If the azimuth sampling is viewed as a spoke density, then in this case, the spokes or acoustic rays are 0.75° apart. Small spatial events that consist primarily of high spatial frequencies relative to the spoke density will be missed. Furthermore, since the acoustic field is viewed through a finite window (the transducer) there is a resolution limit related to the transducer aperture and the acoustic wavelength. For this reason, it makes no sense to increase the spoke density if the aperture-related resolution does not justify it.

Scan Conversion Methods

Digital scan conversion is a relatively recent innovation in ultrasound imaging. Earlier systems used direct analog converters to modulate the intensity of an X-Y display. There are problems with this technique that outweigh its simplicity. First, a completely analog conversion results in a picture that looks like spokes of a wheel with an image superimposed on it. By today's standards, this is unacceptable image quality. Also, because storage of the data in a digital memory allows high-quality freeze-frame display and the ability to manipulate the image using various gray-level mapping curves and digital enhancements, analog conversion is no longer a viable option for medical ultrasound imaging.

Many digital scan conversion methods have been described[1] that map polar coordinate data to a rectangular format, but most of these suffer digital artifacts caused by the scan conversion process. To review some of these methods, the term scan conversion is used here to refer to the spatial transformation process by which data that naturally occurs in a polar coordinate system is mapped into a rectangular memory or grid. The problem is that the precise loca-

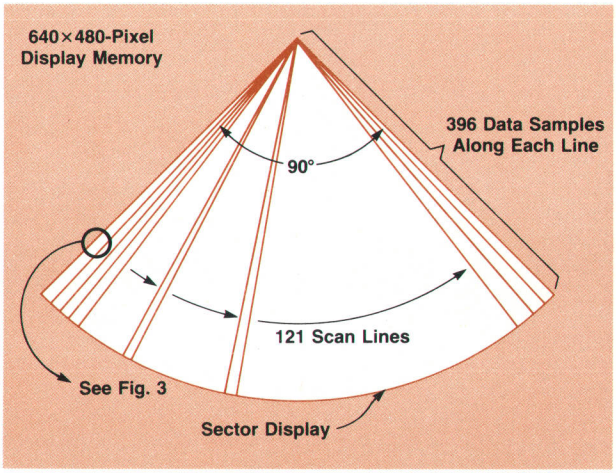

Fig. 1. *The display of a 90° acoustic sector scan is accomplished by mapping the 121 scan lines, each containing 396 data samples, onto the HP 77020A Ultrasound Imaging System's 640×480-pixel display memory as shown. A magnified view of the encircled area is shown in Fig. 3 to illustrate the mapping problem.*

tion of each sample point in space does not, in general, correspond to an allowable display point. Therefore, the data must be adjusted or scan converted before it can be written to the display memory.

The typical digital scan converter maps the scanner data to the nearest display memory location, that is, the polar coordinates are converted to rectangular coordinates, which in turn are quantized to the nearest pixel (display point). Each ray or scan line maps to the memory grid in a somewhat irregular fashion. For example, portions of the data from neighboring lines can overwrite each other. The resulting image appears as a series of straight line segments. This basically incorrect process, where the data is pushed and pulled into alignment with the memory grid, results in an annoying artifact called a Moiré pattern, which is a well-defined pattern of holes in the image corresponding to the unaddressed pixels (Fig. 2a). This pattern is often reduced by creating interpolated scan lines between the actual scan lines and converting these in an identical manner. However, the overwriting problem then becomes more severe. Another method fills the holes by horizontally smearing immediately adjacent data into each hole to complete the scan conversion (Fig. 2b), but this introduces other artifacts. Hence, most of the current scan conversion methods create an image with a "steppy and blocky" appearance.

R-Theta Scan Conversion

The 77020A's R-Theta scan conversion method uses a real-time reconstruction technique. The intensity values for all pixels that lie between two adjacent scan lines are interpolated using Equations (1), (2), and (3).

$$Z_{RI} = Z_{I(n)}(1 - R_{ERR}) + Z_{I(n+1)}R_{ERR} \quad (1)$$

$$Z_{RO} = Z_{O(n)}(1 - R_{ERR}) + Z_{O(n+1)}R_{ERR} \quad (2)$$

$$Z = Z_{RO}(1 - \Theta_{ERR}) + Z_{RI}\Theta_{ERR} \quad (3)$$

These equations result from the evaluation of the generalized interpolation formula

$$Z(r,\Theta) = \sum_j \sum_k S(r - j\Delta r,\ \Theta - k\Delta\Theta)Z(j\Delta r, k\Delta\Theta) \quad (4)$$

where the interpolation function $S(r,\Theta)$ takes on the specific form of a two-dimensional triangular function. $Z(j\Delta r,k\Delta\Theta)$ corresponds to an actual sample value and $Z(r,\Theta)$ is an interpolated value at the pixel site. Equations (1), (2), and (3) are best explained by referring to Fig. 3. $Z_{O(n)}$ and $Z_{I(n)}$ are equivalent samples (in a radial sense) on two adjacent scan lines with $Z_{I(n)}$ representing the sample on the line with a shallower angle from the normal to the transducer.

Equation (1) radially interpolates a new value Z_{RI} between the inner and outer sample points on the inner radial line based on the radial position of the selected display point (Z in Fig. 3). Equation (2) performs the same interpolation on the outer radial line (Z_{RO}). Equation (3) linearly

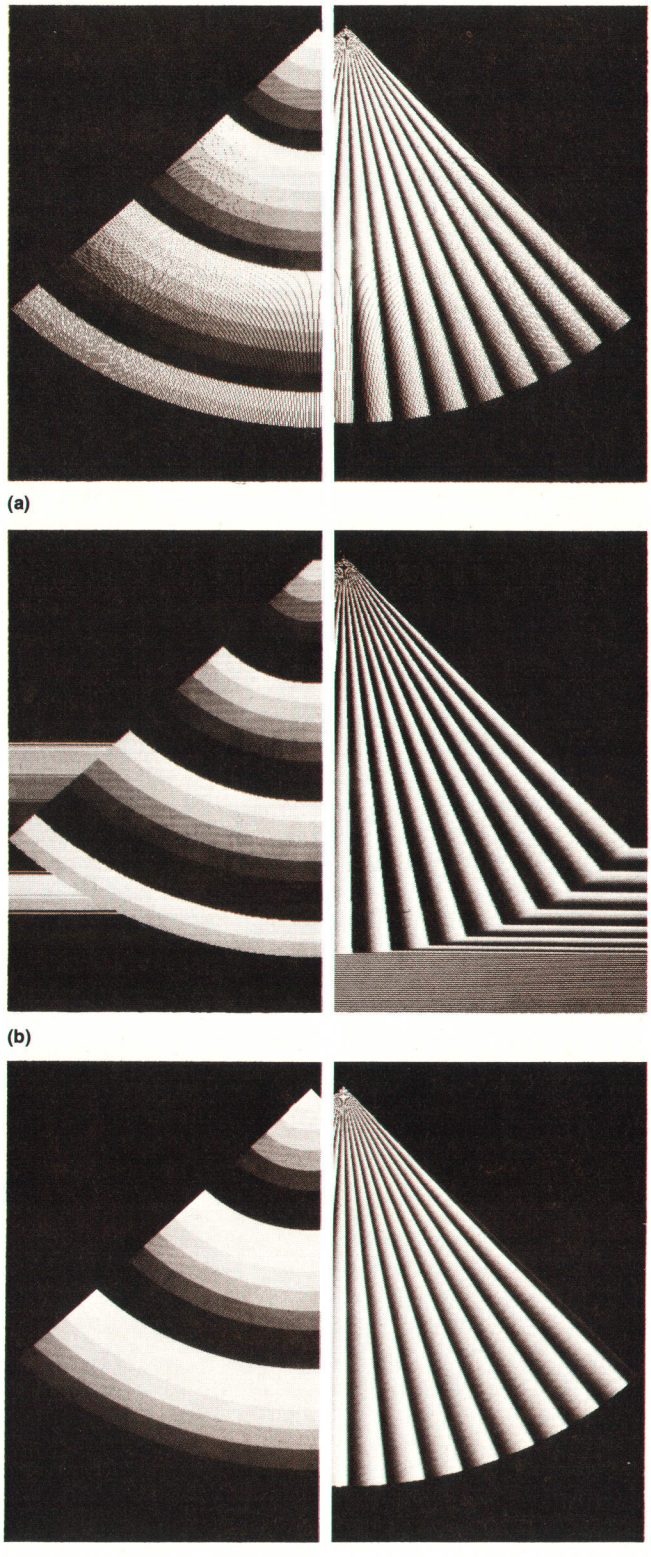

Fig. 2. *Comparison of displays resulting from (a) a commonly used scan conversion algorithm, (b) horizontal fill-in enhancements to the process used for (a), and (c) the R-Theta conversion algorithm used in the 77020A. The left half shows half of a concentric ring image and the right half shows half of a radial spoke image. Note the Moiré pattern present in (a) and the stepped lines in (b).*

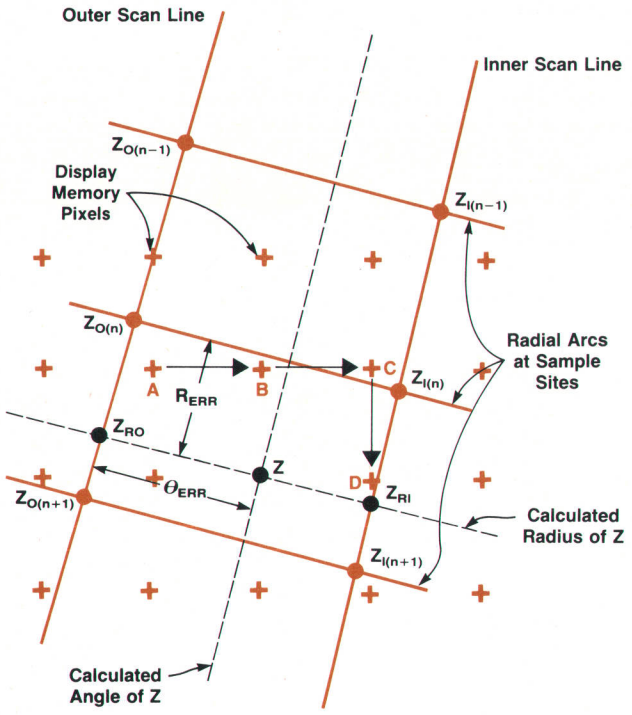

Fig. 3. *Enlarged view of a portion of one slice of the sector. The dots represent data samples received from the scanner and the crosses represent the display pixels the data samples are to be mapped to. See text for additional explanation.*

interpolates Z_{RI} and Z_{RO} in the azimuth (Θ) dimension in a similar manner to assign the proper value to the display point at Z. The 77020A's digital scan converter uses this interpolation algorithm to assign values to all of the display points bounded by two successive scan lines. The process is repeated for all scan lines in the displayed sector.

Hardware Design

The block diagram in Fig. 4 details the circuitry involved in implementing the R-Theta scan conversion.

Input Buffers and Multiplexers. Since each radial scan line is received from the 77020A's scanner in an asynchronous fashion, the sync/latch function is nothing more than a digital resynchronization. Each data or header word is accompanied by a strobe which indicates when that word is valid. The word rate, and hence the strobe frequency, varies with imaging depth, but never exceeds 3.8 MHz. The strobe is sampled at 12 MHz, and when found true, the remaining eleven data lines are latched and then interpreted.

One of the lines, the format bit, indicates whether the word is a header (line number information) or a data word. If it is a header word, a new scan line is imminent. Thus, the digital scan converter must be finished with the line it was processing. Also, the remaining bits of the header word indicating the line number (angle of the scan) must be placed into the 3-header FIFO (first in, first out) buffer for future use. In addition to indicating the start of a new line, the header word indicates the end of the previous line, and therefore causes the rotating 3-line data buffer to rotate, putting the currently filling buffer into read mode and preparing the buffer with the "oldest" data to receive data. Receiving a header word causes a line number to pop out of the 3-header FIFO buffer. This line is processed next by the digital scan converter. The R-Theta error calculators are reset to zero and the X and Y address counters are preset to a processor-selectable "origin." Finally, the X-Y raster state machine is reset to the apex of the scan slice and the new line number from the 3-header FIFO buffer is passed to the R-Theta error calculator and the X-Y raster state machine, which need angular information to perform their functions.

The rotating 3-line data and 3-header FIFO buffers work in concert so that, as a new line number is emerging from the FIFO, the data for that scan line is also emerging from the rotating buffers. These provide the three levels of delay necessary to interpolate between two scan lines, because the header word cannot be processed immediately when it is received, but rather must be delayed for two line periods while the data is gathered. The 3:1 multiplexers are used to select the inner and outer lines for input to the 8-stage shift registers.

The dual 8-stage shifters are essentially a cache memory, retaining the last eight data samples from each of the two lines for which the slice is being interpolated. These bidirectional shift registers allow sequential recall of previous data samples. The first two stages of each shifter provide the inner sample (closest radially to the sector origin) and the outer sample (more distant) for each of the lines. Thus, the outputs of the shifters are the four sample values that surround the display pixel for which an interpolated value is sought. As the slice rastering progresses from pixel to pixel, two signals cause the shifters either to receive the next sample from the buffers (INCR) or to back up to retrieve a previously used sample (DECR). Of course, the buffers must also back up when DECR is true or advance when INCR occurs. It may not be obvious why it is necessary sometimes to retrieve old data samples. Referring to Fig. 3, which represents a slice near the 45° line on the left side of the sector, it can be seen that as the raster path traverses from pixel A to pixel B, and then to C, an integral radial boundary (represented by the arc from $Z_{O(n)}$ to $Z_{I(n)}$) is crossed. Hence, the four samples surrounding pixel C are not the same as those surrounding pixels A and B. The same situation holds true for the right side of the sector and for all scan lines with steep angles.

To handle this situation, each time an integral radial boundary is crossed, an INCR or DECR is generated, depending on the direction of the crossing. If the raster crosses in a direction that decreases the radius of the slice, for example from pixel B to pixel C in Fig. 3, DECR is true and the shifters are left shifted, retrieving samples $Z_{I(n-1)}$, $Z_{I(n)}$, $Z_{O(n-1)}$, and $Z_{O(n)}$ to provide the new correct corner values. Samples $Z_{I(n+1)}$ and $Z_{O(n+1)}$ are purged from the shifters by being shifted out the left end into a bit bucket. However, the rotating buffers have also backed up so that $Z_{I(n+1)}$ and $Z_{O(n+1)}$ are now present on their outputs.

When the raster scan passes from pixel C to pixel D, the radial boundary is crossed in the other direction, yielding an INCR. The shifters shift right, dropping $Z_{I(n-1)}$ and $Z_{O(n-1)}$ out the right end, and the rotating buffers now make $Z_{I(n+2)}$ and $Z_{O(n+2)}$ available at their outputs. Out of the first two shifter stages now come $Z_{I(n+1)}$, $Z_{I(n)}$, $Z_{O(n+1)}$,

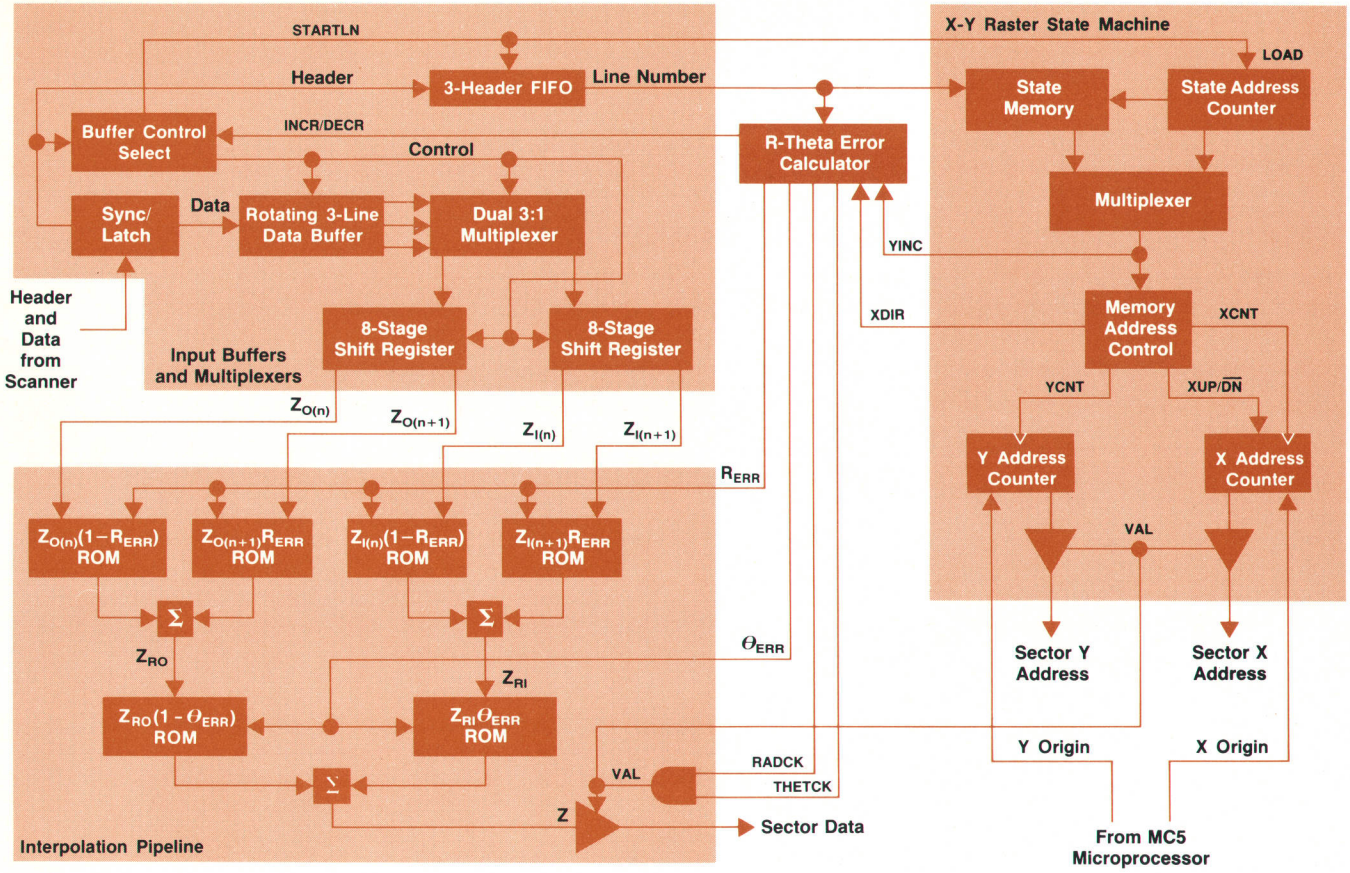

Fig. 4. *Block diagram of the R-Theta scan conversion system.*

and $Z_{O(n)}$, which represent the four samples surrounding pixel D (as well as pixels A and B earlier).

X-Y Raster State Machine. The interpolation starts with a large state machine programmed to scan from the apex of the slice down to the slice's outer radial limit in a predetermined way. Each slice has a unique traversal path selected to minimize addressing pixels not lying in the currently addressed slice and to simplify encoding. EPROMs store the encoded traversal paths and the paths used for the left half of the sector are reflected by symmetry into its right half.

By using an extremely simple encoding algorithm, each EPROM can store eight slice traversal paths. With the slice traversal always beginning at the apex, a logic one indicates a drop in the Y direction and a logic zero indicates movement in either X direction. Note that only Y increments are used; X addressing is made bidirectional by using an additional flag bit XDIR, which toggles every time a movement in Y is made. The XDIR flag is set to one at the apex to indicate that the next X movement is outward to the outer scan line. This holds true for slices on both sides of the sector because of the definitions used for inner and outer scan lines.

A STARTLN signal generated by a header word from the scanner initializes the state address counter. The output of this counter and the line number form the address for the EPROMs. The traversal bytes are read by the state address counter indexing through the 256-byte address space for that particular line number. The three least-significant bits of the state address counter serialize the byte data to form the YINC signal. Asserting YINC causes the memory address control to increment the Y address counter with a YCNT signal. Deasserting YINC generates an XCNT signal, which is coupled with XDIR to form XUP/$\overline{\text{DN}}$, which increments or decrements the X address counter.

The X and Y address counters are loaded after every STARTLN signal with the sector origin as specified by the microprocessor. This positions the sector data within the digital scan converter's 640×480 memory space since all pixel movements dictated by the state memory are relative to the apex. Although this accounts for how the address counters sequence in a raster-like manner down through each slice, the interpolation pipeline still must be told in some manner which samples are to be used for interpolating and what the interpolation weights are.

The error weightings R_{ERR} and θ_{ERR} are necessary to use interpolation equations (1), (2), and (3). Since the radius and angle of each sample is known from its header word and sample number, the straightforward approach is to calculate the polar coordinates of each pixel site within the sector. Then, with a little comparison circuitry between the pixel polar coordinates and the sample polar coordinates, the values for R_{ERR} and θ_{ERR} could be calculated. Using the apex as the reference point for the rectangular coordinates, the equations that must be solved for every pixel addressed by the state memory are

$$R_p = \sqrt{X_p^2 + Y_p^2} \quad (5)$$

$$\Theta_p = \tan^{-1}(X_p/Y_p) \quad (6)$$

R-Theta Error Calculator. Because a new pixel is addressed every 160 ns, simplifications were implemented in hardware to calculate pixel polar coordinates R_p and Θ_p. These calculations are performed by the R-Theta error calculator. The inputs are the line number, YINC, and XDIR. The outputs are R_{ERR}, Θ_{ERR}, VAL, INCR, and DECR. R_{ERR} and Θ_{ERR} are fed to the interpolation pipeline for calculating the interpolated data value. They represent the radial and angular distances between the currently addressed pixel and the innermost sample on the outer scan line. They are shown in Fig. 3 where $Z_{O(n)}$ is the reference. VAL is used to qualify the pixel as being within the slice bounds, that is, its radius and angle information satisfy the currently addressed slice.

Interpolation Pipeline. Once R_{ERR} and Θ_{ERR} are determined and the four values, $Z_{I(n)}$, $Z_{I(n+1)}$, $Z_{O(n)}$, and $Z_{O(n+1)}$, are also available, the interpolation takes place. The interpolation pipeline, although requiring significant hardware, is a very straightforward process. The four corner values are radially interpolated to yield two intermediate values, Z_{RI} and Z_{RO}, according to Equations (1) and (2). Then the final value Z corresponding to the gray level assigned to the associated display pixel is determined by Equation (3).

The final step is to write Z to the correct address in the display memory. This operation is regulated by VAL, which as explained earlier, is true only when the pixel is within the slice. If the pixel is not in the slice, but was in the slice traversal path, VAL is false, disallowing the final write to the display memory.

The scan conversion system's pipelined architecture interpolates a new pixel every clock cycle (160 ns). A typical slice is composed of 1026 pixels, and a 90° sector contains about 123,000 pixels. Each of these is interpolated once every video frame (16.7 ms). Fig. 2 illustrates the improvement in image quality gained by using the R-Theta algorithm.

Reference

1. J.Ophir and N.F. Maklad, "Digital Scan Converters in Diagnostic Ultrasound Imaging," *Proceedings of the IEEE*, Vol. 67, no. 4, April 1979.

Ultrasound Image Quality

by Richard A. Snyder and Richard J. Conrad

IMAGE QUALITY is a measure of the diagnostic utility of an ultrasound image to a physician. Generally the physician uses ultrasound to examine the internal organs of a patient noninvasively. Hence, the ultrasound image must be an accurate representation of structures in the body.

The human body is an ultrasonic medium that is far from ideal in its ability to propagate an undistorted ultrasound wave, because the body attenuates, scatters, and refracts the ultrasound wavefront. The factors influencing the quality of the ultrasound image include resolution, depth of penetration, and tissue representation.

Resolution

The resolution of the ultrasound image is a measure of its ability to separate closely spaced individual structures. Referring to Fig. 1, the resolution for a phased-array sector scanner is divided into three distinct areas: the resolution in the direction of the scan angle, or azimuth resolution, the resolution in the direction perpendicular to the plane of the scan, or elevation resolution, and the resolution in the direction of pulse propagation, or range resolution.

The sector image is formed by transmitting an ultrasound pulse of a particular center frequency in one direction into the body and receiving and processing its echoes. The direction of propagation defines the position of one scan line of the image while the arrival times of the echoes determine where along that line the echo sources lie. This transmit/receive process is repeated in different directions until the entire plane of the sector has been scanned.

The intensity distribution in space of the transmitted pulse as it propagates is known as the transmit beam pattern. The sensitivity distribution in space of the receiver is known as the receive beam pattern. The total round-trip azimuth resolution and elevation resolution are each determined by the product of these two beam patterns. The distinction between elevation and azimuth resolution is necessary because the aperture of the acoustic transducer is rectangular, with one dimension falling along the elevation direction and the other along the azimuth direction. These dimensions are not necessarily equal in length, so the round-trip beam patterns in the azimuth and elevation directions may be different. Each beam pattern is a function of the aperture size, the wavelength of the ultrasound pulse, and the focal distance of the acoustic lens. Because the aperture size is typically only 32 times the wavelength, or less, diffraction effects play a significant role in the analysis of the beam pattern. The first-order diffraction effect causes

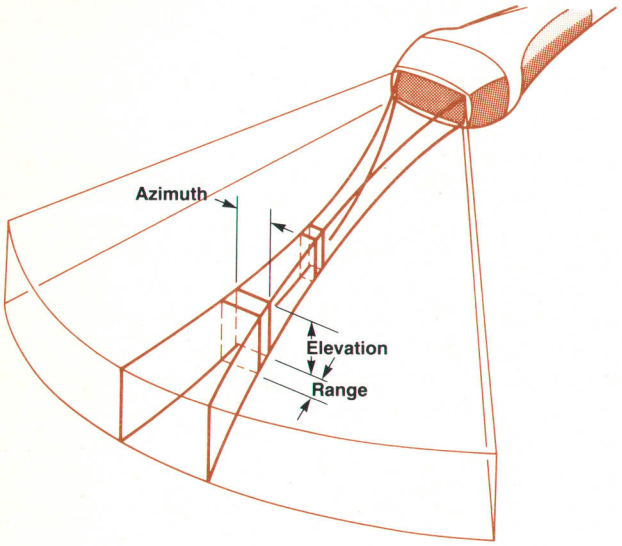

Fig. 1. *An ultrasound image for a 90° sector is obtained by scanning a beam of ultrasound pulses in an azimuth direction. The beam's azimuth, elevation, and radial resolutions are functions of many factors as discussed in the text.*

the beam to diverge in the transducer's far field. The far field region begins at a distance $Z = W^2/\lambda$ for a rectangular aperture, where W is the aperture size and λ is the wavelength. In the near field, the beamwidth may be reduced by focusing with a lens or focusing by controlling the phase of each element in the phased array. The beamwidth at the focal point may be reduced and the near field extended by increasing the aperture. The price of this improvement in resolution at the focal point is that the beamwidth before or beyond the focal point increases rapidly with aperture causing a shorter depth of field. In fact, although beamwidth at the focal point decreases linearly with aperture size, depth of field decreases with the square of the aperture size. This same loss in depth of field is experienced when the focal point is brought closer to the aperture. This situation forces a compromise between resolution at the focal point and depth of field whenever a fixed focus is used. Fig. 2 illustrates the approximate transmit beam patterns from transducers with apertures of equal size, but with four different focal points. Although the minimum width of each beam pattern does decrease as the focal point is moved toward the transducer, the beamwidth diverges more rapidly away from the focal point.

For the phased-array scanner, the transmit focal point in the azimuth direction is controlled by the delay applied to each element of the array when the pulse is transmitted. This focal point is fixed at a depth that provides the best compromise between depth of field and focal point beamwidth for each type of transducer. The transmit focal point in the elevation direction is controlled by a fixed-focus cylindrical acoustic lens. The lens is oriented such that it does not affect the azimuth focus. Hence, the elevation and azimuth focal points can be chosen to be different.

Like the transmit focal point, the receive focal point in the azimuth direction is controlled by the delay given to each element of the phased array. A basic difference is that because the echoes from increasing depths are received over a period of increasing time, the receive focal point can be controlled to track the depth from which the echoes are returning dynamically. This dynamic focusing eliminates the depth of field problem associated with a fixed focus.

The effect of dynamic focusing on image quality can be seen by comparing two images of a test target or "phantom" (Fig. 3). This phantom contains a series of nylon wires and cystic regions imbedded in a tissue-mimicking medium. The size of the wire images and the clarity of the round cysts provide a measure of azimuth resolution. In the first image the dynamic focusing is disabled and the receive focal point is fixed at 8 cm (Fig. 3a). In the second image the dynamic focusing is enabled, providing optimum beam width along all the scan lines (Fig. 3b).

The effect of elevation resolution on image quality is not as directly apparent as the effect of azimuth resolution. Elevation resolution determines the thickness of the sector image plane. All echoes within this plane are mapped together into the two-dimensional image. A thick image plane results in the obscuring of some small details. The image may still look sharp, but some information is lost. Consider an image of a small vessel in the body parallel to the plane of the scan. The cross section of the vessel should appear as a narrow black void because the blood within the vessel returns no echoes. If the image plane is thicker than the diameter of the vessel, then the echoes from tissue above and below the vessel are mapped into the image of the vessel, obscuring it. This effect can be seen in two images of a tissue-mimicking phantom containing cylindrical regions representing horizontal blood vessels (Fig. 4). The images were made with two transducers having different elevation focal points.

Because there is no overall best choice of elevation focal

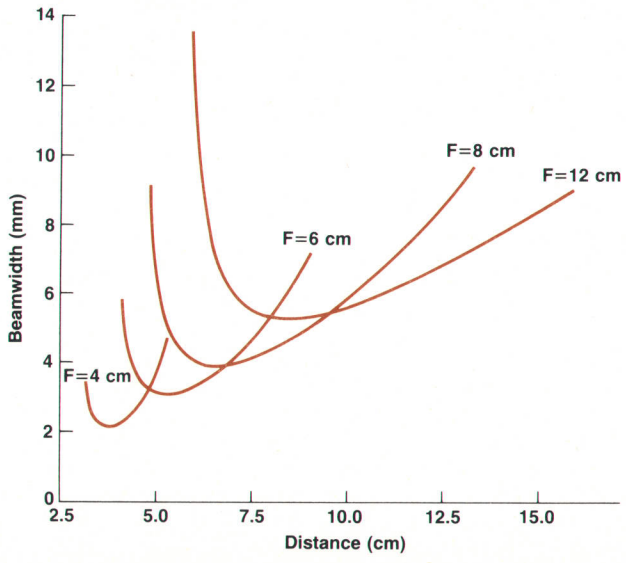

Fig. 2. *Transmit beamwidth versus distance for equal-aperture, 5-MHz transducers with different focal lengths.*

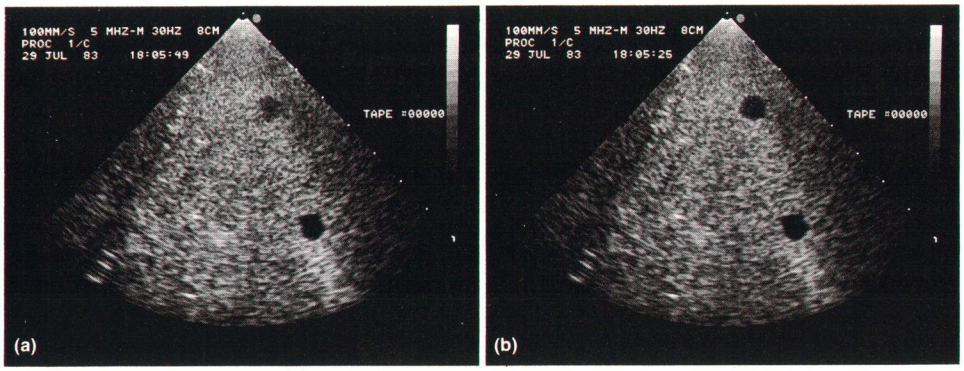

Fig. 3. *Effect of dynamic focusing on image quality. (a) Image using a transducer with a fixed receive focus at 8 cm. (b) Image using a transducer dynamically focused during reception of echoes.*

point, several transducers with different elevation focal points are available for the HP 77020A Ultrasound Imaging System (Table I). Thus, users can select the transducer frequency and focal point most appropriate for their particular imaging application.

Table I

Transducers for HP 77020A Ultrasound Imaging System

Transducer Model	Center Frequency	Elevation Focal Point
21200A	2.5 MHz	12.0 cm
21205A	3.5 MHz	7.5 cm
21206A	3.5 MHz	4.0 cm
21210A	5.0 MHz	6.0 cm
21211A	5.0 MHz	3.5 cm

Range or axial resolution is a measure of the ability to resolve individual closely spaced targets along the acoustic beam axis. Axial resolution in a pulsed echo system is determined by system bandwidth and center frequency. Transducers typically have a constant percentage bandwidth, and thus the higher the center frequency of the transducer, the wider the bandwidth and the better the range resolution. The bandwidth of the transducer is not the only consideration. The receiver bandwidth also affects resolution since the time response of the receiver filter can broaden the returning echo pulses. The 77020A minimizes receiver pulse broadening by using a high-frequency IF stage and optimizing filters for each transducer center frequency.

Sidelobe Levels

Another very important aspect of image quality is the effect of sidelobes and grating lobes. Sidelobe and grating lobe artifacts have plagued phased-array systems in the past. Sidelobes appear in an image as lateral streaks emanating from very bright targets. The two images in Fig. 5 illustrate the effect of sidelobes on image quality. The first image was made with sidelobes at a -40 dB level (Fig. 5a). The second image was made with sidelobes at a -60 dB level (Fig. 5b). The effect of the higher sidelobe level is the lateral smearing seen in the first image. Also, the dark blood vessels become filled with "clutter" caused by the higher sidelobes.

The 77020A suppresses the clutter level caused by high-order sidelobes by more than 60 dB and eliminates the grating lobe by setting the transducer element-to-element spacing to a half wavelength.

Depth of Penetration

One fundamental problem in ultrasound imaging is that soft tissue attenuates ultrasound roughly linearly with frequency. The human liver, for example, attenuates ultrasound by about 0.5 dB/MHz/cm. Thus, a 2.5-MHz pulse propagating round-trip through 40 cm of liver tissue is attenuated by 50 dB and a 5.0-MHz pulse is attenuated by 100 dB. For this reason, deep imaging is usually done with lower-frequency transducers and shallow imaging is done with higher-frequency transducers to take advantage of their superior image quality. It will be shown later that a higher acoustic frequency does more for the image than just provide better range resolution.

Frequency-dependent attenuation has an adverse effect on the spectrum of the transmitted pulse. Because high

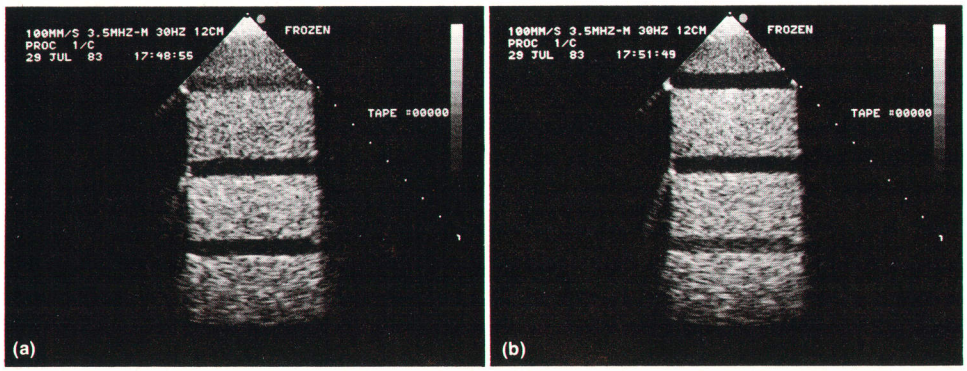

Fig. 4. *Effect of transducer's elevation focal point on image quality. (a) Image with an elevation focal point at 8 cm. (b) Image with an elevation focal point at 4 cm.*

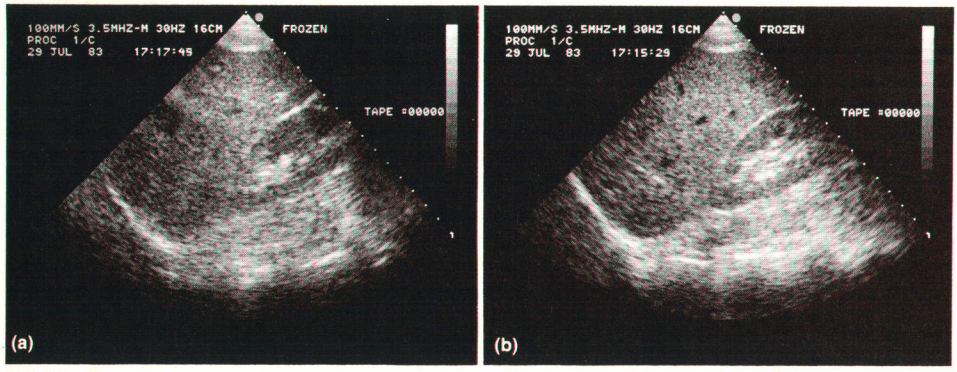

Fig. 5. *Effect of transducer sidelobe level on image quality. (a) Image with sidelobe level at −40 dB. Note the lateral smearing. (b) Image with sidelobe level at −60 dB.*

frequencies are attenuated more than low frequencies, the center frequency of the transmitted spectrum is shifted down as the pulse propagates. Fig. 6 illustrates the shift in center frequency of a pulse spectrum at various depths. This shift in center frequency degrades the azimuth resolution because the wavelength of the pulse increases while the aperture size remains fixed. The effect of this spectral shift on image quality is controlled to some extent by the choice of receiver bandwidth. A wide bandwidth allows imaging at greater depths in the body, but with degraded resolution. A narrow bandwidth improves both azimuth and elevation resolution and focusing at the expense of axial resolution.

The 77020A uses a compromise between these two extremes for sector imaging, and uses a wider bandwidth for M-mode where axial resolution is more important. The ability to optimize filtering for each transducer and mode of operation is an important feature of the 77020A System.

Tissue Representation

The ability of an ultrasound imaging system to represent the range of echo amplitudes as different gray levels in the image is another measure of image quality. This representation affects how the separate tissues of the body are seen in the image. Echoes from within the body occur when the propagating ultrasound pulse encounters a change in the characteristic impedance of the body tissues. The characteristic impedance Z is defined as $Z=\rho v$, where ρ is the density of the medium of propagation and v is the velocity of propagation. When the impedance change occurs over a boundary greater than a few wavelengths in extent, such as the boundary between a blood vessel wall and blood or organ tissue, a specular or mirror-like reflection occurs. The intensity I of echoes from these specular reflectors depends upon the reflection coefficient and is given for a boundary that is perpendicular to the direction of propagation by $I=I_s(Z_2-Z_1)/(Z_2+Z_1)$, where I_s is the incident pulse intensity, and Z_1 and Z_2 are the two impedances. Specular echoes are frequency-independent and propagate in a direction that depends upon the orientation of the boundary with respect to the pulse's propagation direction.

Generally the impedance differences between the soft tissues of the body are small enough so that only a small portion of the incident pulse is reflected back to the receiver and the major portion of the pulse continues on to greater depths. However, there are cases where the impedance differences are great and most of the pulse is reflected back. When this occurs, a shadow appears in the image behind

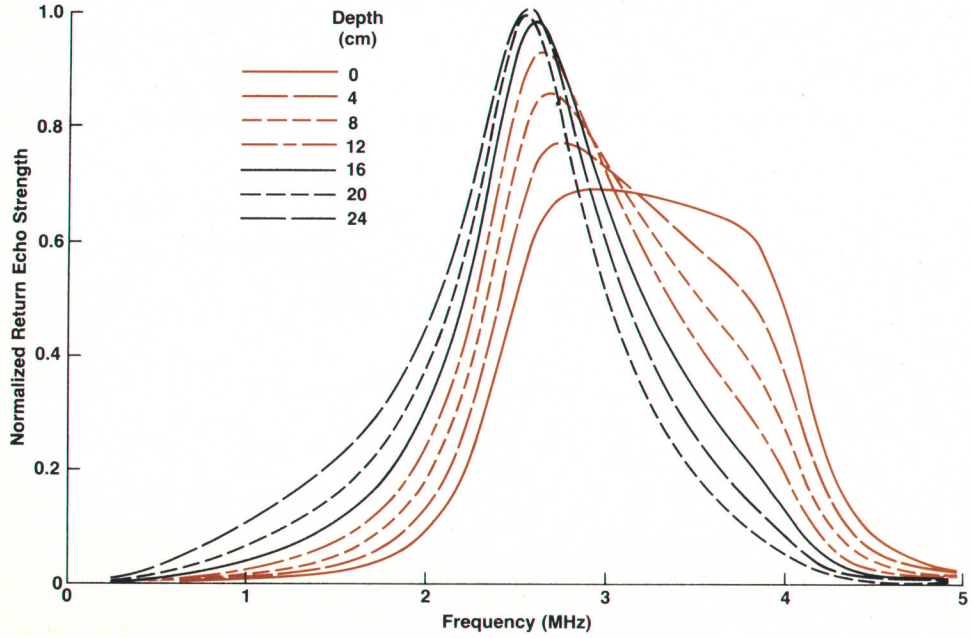

Fig. 6. *Variation with depth of the frequency spectrum of detected ultrasound echoes. The incident pulse spectrum is centered at 3.5 MHz. (An attenuation of 0.7 dB/cm/MHz is assumed.)*

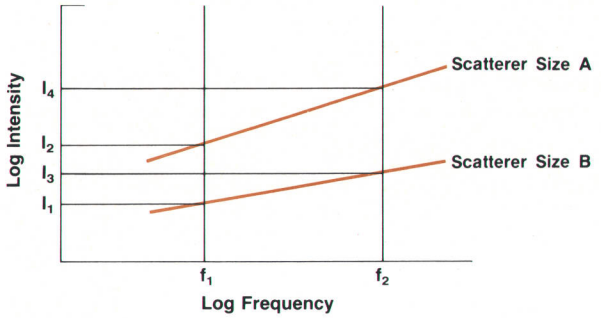

Fig. 7. *Scatter intensity versus frequency for two scatterers of different size. The difference $I_4 - I_3$ between the scatter intensities at frequency f_2 is greater than the difference $I_2 - I_1$ between the scatter intensities at frequency f_1. This result provides greater contrast between regions of tissue that are structurally different on a scale much smaller than the wavelength of the ultrasound pulse.*

the impedance boundary. This effect can be most useful in applications where large impedance changes are abnormal, such as a calcification or gallstone in the gall bladder. The strong shadow behind a gallstone is often taken as evidence confirming its presence.

When the region of an impedance change extends over less than one wavelength, part of the incident pulse is scattered in all directions according to Rayleigh scattering. The intensity of the scattered pulse is proportional to the product of the fourth power of the frequency of the pulse and the sixth power of the radius of the region of the impedance change. All soft tissues produce scatter echoes because of their cellular structure and small internal structural details. Some of the scatter propagates back to the receiver and is known as backscatter. When propagating through tissue, the transmitted pulse produces a continuous complex of backscatter echoes that constructively and destructively interfere with one another in a random fashion. The resulting interference pattern seen in the image is known as a speckle pattern or simply as texture (see page 39). The texture intensity of each organ is different and can be used to differentiate organs and to indicate abnormal regions such as tumors within organs.

The ability to show difference in speckle pattern intensities is another measure of image quality. Because of the frequency dependence of the scatter intensity, higher-frequency transducers provide greater differentiation of tissue types. This is shown in Fig. 7 where scatter intensity is plotted against frequency for scatterers of two different radii. The improved tissue contrast detectability of higher frequencies can be seen in a series of three images of a tissue-mimicking phantom containing a region of scatterers made using three different frequencies (Fig. 8). Notice the increase in detectability of the round 20-μm regions with an increase in frequency.

Bandwidth also affects the appearance of the texture pattern. Since texture is caused by the addition and cancellation of randomly received echoes, a narrow bandwidth provides more coherence and produces a coarser texture than a wide bandwidth. The higher the frequency, the finer the texture, and the more filled-in or smoother the image looks, making it easier to identify boundaries between different types of tissues or small vessels.

Once the received echoes are optimally filtered, they must be detected without time-response degradation and presented as gray levels on a CRT display. The different types of echoes from the body cover a dynamic range on the order of 40 to 50 dB. That is, the weakest echoes can be 40 to 50 dB below the strongest echoes from areas of equal depth. Because the dynamic range of images judged to be most pleasing to the eye is about 25 dB, a form of nonlinear processing is used to compress the range of intensities displayed in the image. This process is important to the quality of the image. Subtly different textures must be discernible while large specular echoes must not be too distracting.

Two different methods for controlling the processing of echo amplitudes into image intensities are provided in the HP 77020A Ultrasound Imaging System's scanner. One method controls the blending of the logarithmic and linear versions of the echo amplitude before digitization and storage in memory. This variable blending allows the user to control the amount of echo dynamic range displayed in the image. For example, in abdominal imaging where soft tissue is to be displayed with high-level specular echoes from organ boundaries and bright gas-tissue interfaces, the blend is set to be mostly logarithmic. The other method digitally controls the assignment to gray levels of the digitized echo amplitudes stored in memory. By using post-processing in series with logarithmic compression, the user can fine-tune the image presentation to provide the best differentiation between the tissue types studied.

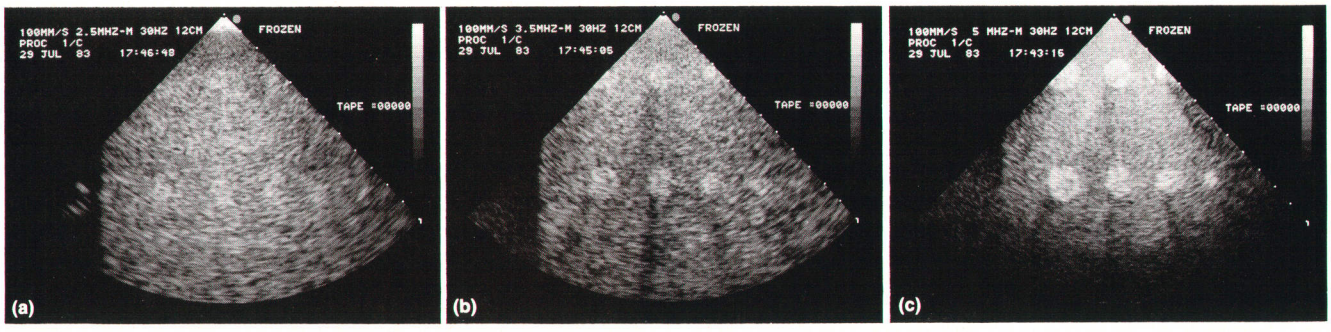

Fig. 8. *Images made of a region of 20-μm diameter scatterers surrounded by 7-μm diameter scatterers using the 77020A System's (a) 2.5-MHz, (b) 3.5-MHz, and (c) 5.0-MHz transducers.*

Coherent Speckle in Ultrasound Images

by Paul A. Magnin

Speckle is the term used to describe the mottling found in ultrasound images. Speckle noise tends to manifest itself as a relatively high-contrast, high-spatial-frequency mask superimposed on the desired ultrasound image. Such noise tends to make subtle differences in the gray levels of different tissues imperceptible and reduces the apparent resolution of the image significantly below the diffraction limit.

The speckle phenomenon is inherent in all coherent imaging modalities. Coherent illumination has the property that the phasors at all points in the field of illumination vary in unison. While any two points in the field of illumination may have different relative phases, the phases of those points change in an identical manner. The most commonly seen speckle is in laser images. In this case the object illuminated with laser light has some surface roughness which is large compared to the wavelength of the laser light. The light returning to the eye of the observer from a particular spot on the object's surface is the complex sum of the light returning from each infinitesimal surface of the tiny resolution area. As long as the observer remains fixed relative to the object, the speckle pattern is stationary. If the observer moves, however, the speckle pattern changes. This motion results in the scintillation the observer sees.

The reason speckle patterns are not observed in ordinary light is a result of the coherence time of the light. Sunlight and common artificial light are coherent, but only on certain time scales. That is to say, the relative phases of the illumination at any two points can vary in unison, but only for a very short time referred to as the coherence interval. If one could make a photograph using ordinary sunlight in a single coherence interval, a speckle pattern would be observed. The human eye, however, averages the swirling speckle pattern to produce an apparently smooth image.

Ultrasound speckle is caused by the constructive and destructive interference of the backscattered echoes. At any given time the echoes returning to the transducer emanate from a resolution volume. The resolution volume size is determined by the transducer dimensions, the ultrasound pulse bandwidth and center frequency, and the degree of focus at the position of interest. The number of scattering sites within a resolution volume is typically very large. These scattering sites are normally individual tissue cells, tissue fibers, and collagenous connective tissue. Each scattering site in this volume produces an echo that can be thought of as a phasor which, when added to the echo phasor from all of the other scattering sites, produces the aggregate echo from that resolution volume. Although the echo from an individual scattering site is too small to be detected at the frequencies typically used for medical imaging, the aggregrate echo from a collection of scattering sites can be detected. If one assumes there are a large number of scattering sites in the resolution volume and that the positions of these scattering sites are randomly distributed with a uniform probability density function, then the amplitude and phase of the aggregrate echo from the resolution volume are random variables. The amplitude of the aggregate echo will be distributed according to a Rayleigh probability density function and the phase of the echo will be distributed according to a uniform probability density function.

As the ultrasound pulse moves through the tissue, the number and orientation of the scattering sites change, thereby changing the value of the complex vector sum of the backscattered echoes. The manifestation of this changing vector sum is the "salt and pepper" appearance of ultrasound images. The random nature of the echo amplitude from tissue makes tissue identification from some form of echo signature very difficult. One cannot assume that a certain tissue will exhibit a characteristic echo. Instead, some form of spatial averaging and statistical analysis or speckle reduction appears to be necessary before tissue signature analysis can be done.

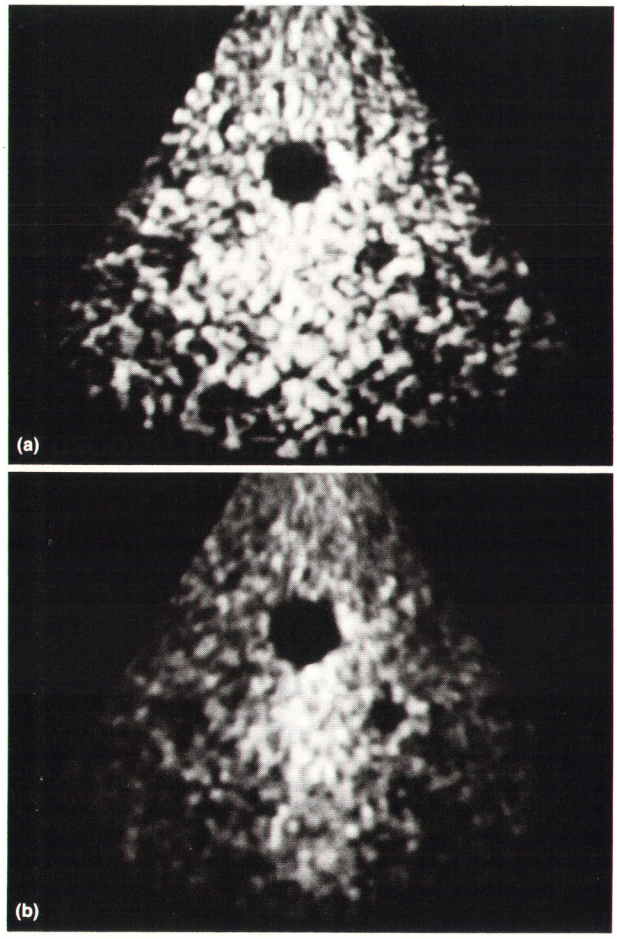

Fig. 1. *Simple image (a) and compounded-frequency image (b) of a tissue-mimicking phantom made on a research phased-array scanner.*

A second vehicle responsible for the mottled appearance of ultrasound images is the presence of inhomogeneous material which acts as an aberrating lens and results in some degree of phase cancellation. This effect can be thought of as being analogous to looking through a translucent shower curtain. If one makes an image of a single point scatterer through an inhomogeneous medium, the phases of the echoes returning to each element of the transducer are disturbed from the spherical phase front one would otherwise expect. The resulting focused and detected echo has a randomly distributed amplitude.

One problem in medical imaging is that some clinicians have a tendency to associate the speckle pattern with the tissue pathol-

ogy. Although the speckle is a result of scattering in the tissue, the pattern itself is also a function of the imaging system. For example, the size of the "speckles" is related to the size of the resolution volume. The resolution volume in turn is related to the transducer's aperture size, pulse frequency and bandwidth, the apodization, and the nature of the subsequent signal processing. It is hard to imagine that any such pattern, which is so easily altered by imaging system parameters, could be considered a function of the tissue alone. Optical texture is commonly thought of as a surface variation with large spatial dimensions compared to the resolution of the imaging system. Similarly, if an analogous ultrasound texture is to be examined, it is necessary to minimize the effects of speckle and to look at surface variations that are larger than the resolution volume of the imaging system.

Two common approaches exist for reducing the amount of speckle artifact present in coherent images. The first involves spatially low-pass filtering the image, which smoothes the mottled appearance of the image. However, since the average speckle size is roughly equal to the resolution of the imaging system, the filtering also necessarily degrades the resolution of the system. For most applications this is considered too high a price to pay. The second approach involves varying certain imaging system parameters, which result in movement of the speckle pattern, and averaging the different speckled images. Any parameter that alters the sum of the echoes returning from the tissue will alter the speckle pattern. Phased arrays have an advantage over mechanically steered imaging systems in that the echoes received by the elements of the array are summed to form the image. Different amplitude weightings on the channels making up the array change the beam characteristics and alter the speckle pattern. One could also make images using different frequencies, foci, bandwidths, compression, or any combination of these parameters. If the different imaging conditions selected produce independent or uncorrelated speckle patterns, upon summation the resultant composite image will exhibit a speckle contrast reduction of $1/\sqrt{N}$, where N is the number of images used to form the composite. Since fixed, resolvable structures remain in the same position for each of the N images, their visibility relative to the speckle noise increases and no degradation of the system resolution occurs. Such images could be obtained in either a serial or a parallel fashion. The disadvantage of the serial implementation is the blurring of rapidly moving structures such as heart valves. A parallel implementation eliminates blurring but requires increased system complexity and cost.

One imaging system parameter which has been varied for the purpose of reducing speckle is the excitation burst center frequency.[1] In this scheme, referred to as frequency compounding, the transducer is excited with a gated sinusoid. Each successive frame is made using a different sinusoidal burst excitation frequency. This is repeated for N different excitation frequencies and the N video frames are summed or averaged visually by the eye of the observer. Significant decreases in the speckle artifact can be obtained using this scheme. Fig. 1 shows two images of a tissue-mimicking phantom made on a research scanner. Fig. 1a is a conventional phased-array image showing a large cyst in the center and a smaller, barely visible cyst below and to the right of the large cyst. Fig. 1b is a frequency compounded image made using five different excitation frequencies. The speckle contrast is significantly reduced, leaving the cyst borders more clearly delineated. Furthermore, the small cyst is more clearly seen. Further reductions in the speckle contrast using similar techniques are necessary if more subtle differences in tissue texture and character are to be determined.

Tissue Characterization

One potential diagnostic advantage of ultrasound imaging is its ability to differentiate between normal and pathological tissue. Presumably pathological tissue exhibits a different texture from normal tissue. Although one major difficulty in discerning subtle differences in tissue texture is the superimposed speckle artifact, it is possible that the speckle pattern itself may prove to be useful diagnostically. One could imagine cases where tissue fibers are organized in some systematic fashion. Speckle from such a tissue matrix would have a regular pattern and an orientation sensitivity. This is analogous to Bragg diffraction found in crystalline structures. However, to date, such tissue regularity has not been demonstrated.

One of the most promising indicators of tissue character has been the slope of the attenuation coefficient versus frequency.[2] Tissues tend to have attenuation characteristics that increase linearly with frequency. Recent studies suggest that an infarcted myocardium has a significantly different slope of attenuation versus frequency than a healthy myocardium. Again it is necessary to account for or minimize the effects of speckle. Tissue characterization by ultrasound would provide a new dimension of diagnostic information. Rather than simply obtaining structural information, ultrasound has the potential for imaging pathology. Ultimately it may be possible to determine the location, severity and type of a tumor or cyst noninvasively, and thereby enhance the diagnostic utility of ultrasound images.

References

1. P.A. Magnin, O.T. von Ramm, and F.L. Thurstone, "Frequency Compounding for Speckle Contrast Reduction in Phased Array Images," *Ultrasonic Imaging*, Vol. 4, 1982, pp 267-281.

2. M. O'Donnell, et al., "Ultrasonic Attenuation in Normal and Ischemic Myocardium," *Ultrasonic Tissue Characterization II*, M. Linzer, editor, National Bureau of Standards Special Publications, U.S. Government Printing Office, Washington, D.C., 1979.

Hewlett-Packard Company, 3000 Hanover Street, Palo Alto, California 94304

Bulk Rate
U.S. Postage
Paid
Hewlett-Packard
Company

HEWLETT-PACKARD JOURNAL

OCTOBER 1983 Volume 34 • Number 10

Technical Information from the Laboratories of Hewlett-Packard Company

Hewlett-Packard Company, 3000 Hanover Street
Palo Alto, California 94304 U.S.A.
Hewlett-Packard Central Mailing Department
Van Heuven Goedhartlaan 121
1181 KK Amstelveen, The Netherlands
Yokogawa-Hewlett-Packard Ltd., Suginami-Ku Tokyo 168 Japan
Hewlett-Packard (Canada) Ltd.
6877 Goreway Drive, Mississauga, Ontario L4V 1M8 Canada

CHANGE OF ADDRESS: To change your address or delete your name from our mailing list please send us your old address label. Send changes to Hewlett-Packard Journal, 3000 Hanover Street, Palo Alto, California 94304 U.S.A. Allow 60 days.

5953-8516